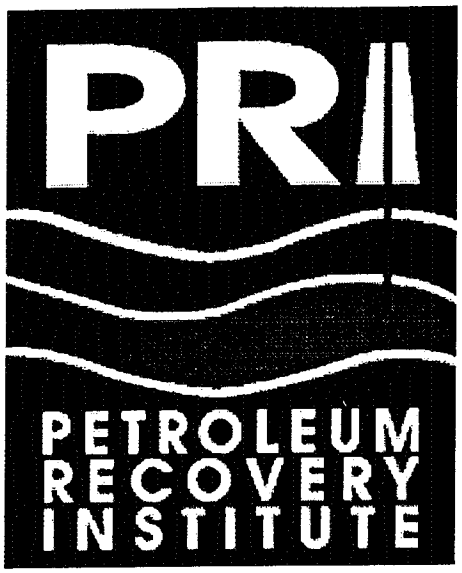

Gas Miscibility and Interfacial Properties Study Using the PRIme™ Method For Statoil

October 1998

Project Team

Douglas Fisher and Marcel Girard

Confidential

Introduction

Interfacial tension (IFT) is measured by either pendant drop or sessile drop. wettability is determined by either contact angle or degree of adhesion (Note: a contact angle of zero, means the solid surface is totally wetted by the non-drop phase).

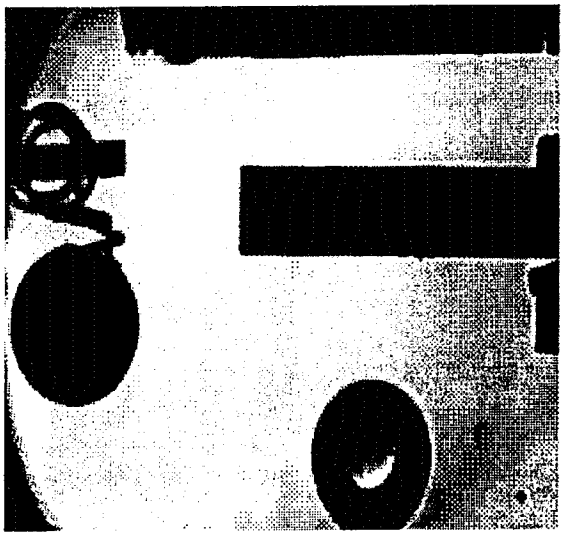

Figure 1

In the case of wettability it is important to state which phase is the initiating phase to contact the solid surface. This is important because to wet the surface, the drop must displace the initial phase (initiating) and then bond to the surface through a chemical /physical reaction. Typically, the aqueous phase is the initiating phase and the oil phase are the drops.

Since the fluids used are complex samples containing a mixture of compounds it should be noted that the image analysis methods used to compute the IFT are complex and produce the best value possible from systems which are of poor optical quality.

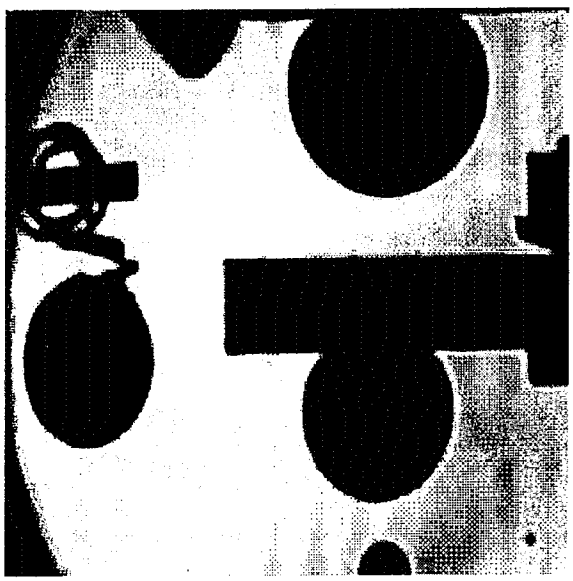

Figure 2

The IFT computations are carried out using the axis symmetric drop shape profile (ADSA-P) method. This method gives good results for both pendant and sessile drops. When the drops are of poor quality we use software and methods developed at PRI (Fisher) to find the best estimate of the drop shape co-ordinates to be used in the ADSA-P model.

In Figure 1 we show an example of a good pendant drop shape and in Figure 2 we show a good sessile drop shape. On the left side of both images you can see an object connected by a wire to a tube. This is the calibration sphere, it is made of synthetic ruby and has a known dimension (0.47 cm). The sphere in the

image appears as an ellipse. The reason for this is that the images are digitized using a system which uses rectangular pixels with an aspect ratio of 1.25. When rectangular pixels are displayed on a system which uses square pixels the objects appear shorter in the X dimension by this ratio.

When we calculate the physical dimensions of the drops we must convert the X co-ordinates by a factor which contains not only the aspect ratio but a conversion for pixels to centimeters. Because we need both an X and Y calibration factor we must use the co-ordinates from the ruby sphere to compute this information. We make use of the fact that the equation for an ellipse gives us both dimensions at once. We fit the co-ordinates of the sphere to this equation by leastsquares. This gives us the best estimate of the conversion factors and the aspect ratio simultaneously. If the fluids are turbid or have a high molar absorbtivity we must use special image analysis techniques to find the edge co-ordinates for both the sphere and the drops. These methods allow us to calculate IFT values under extreme conditions when the more traditional methods fail.

Results

Measurements of IFT were made over a range of pressures using the supplied live oil sample (15/9-19A), using both CO_2 and the supplied hydrocarbon mixed gas. The Figures 1-a to 17-a are the data for the mixed gas whereas the Figures 1-b to 16-b are for the CO_2.

In the case of the mixed gas we observed that the decline rate for the apparent IFT Vs Pressure did not follow the traditional pattern(Figure 2-a), here we see that there is a jump around the 37MPa mark, this change needs some further discussion.

You will notice that in all of the images at all of the pressures we see some streams of oil dissolving in the gas phase. This represents stripping of the light ends from the oil by the hydrocarbon gas. If the oil has any significant concentration of heavy components these will be enriched in the sample and the apparent IFT will be higher than expected. The discontinuity observed in the graph is the result of sampling rate not any smooth functional relationship, although the lines are calculated by nonlinear leastsquares so that all of the data was used to define the decline slope in order to estimate the intersection point. We feel that the value of this intersection is elevated due to the enriching process. In other words the miscibility process is continuos over pressure rather than rapid at or after a given pressure.

In the case of the CO_2 we see the same effect but magnified. The degree of miscibility is much higher than the mixed hydrocarbon gas, even at the first pressure which is quite near the bubble point. Since the extraction process is rapid and large the drops are distorted in shape and as such the calculated apparent IFT has a much larger error band. So even though the graph indicates a simple straight line (Figure 2-b) we feel that this value is also elevated from what is probably the best estimate of the minimum miscibility pressure. We also observed the same enrichment process in this mixture as well.

The image sequence shown in Figures 8-b to 13-b represent a series of drops appearing at slower and slower rates. This allow for longer and longer extraction periods and as such more and more heavy component left on the tip. This is especially obvious in the sequence starting at 14-b. Here we show the extraction process in more detail, and then allow it to end in a stable higher IFT drop which stays on the tip for some time ending in the shapes shown in Figure 15-b. It is clear that the bulk of the oil is extracted early on and the remaining material is not miscible at these pressures and will not be miscible for some significant increase in pressure.

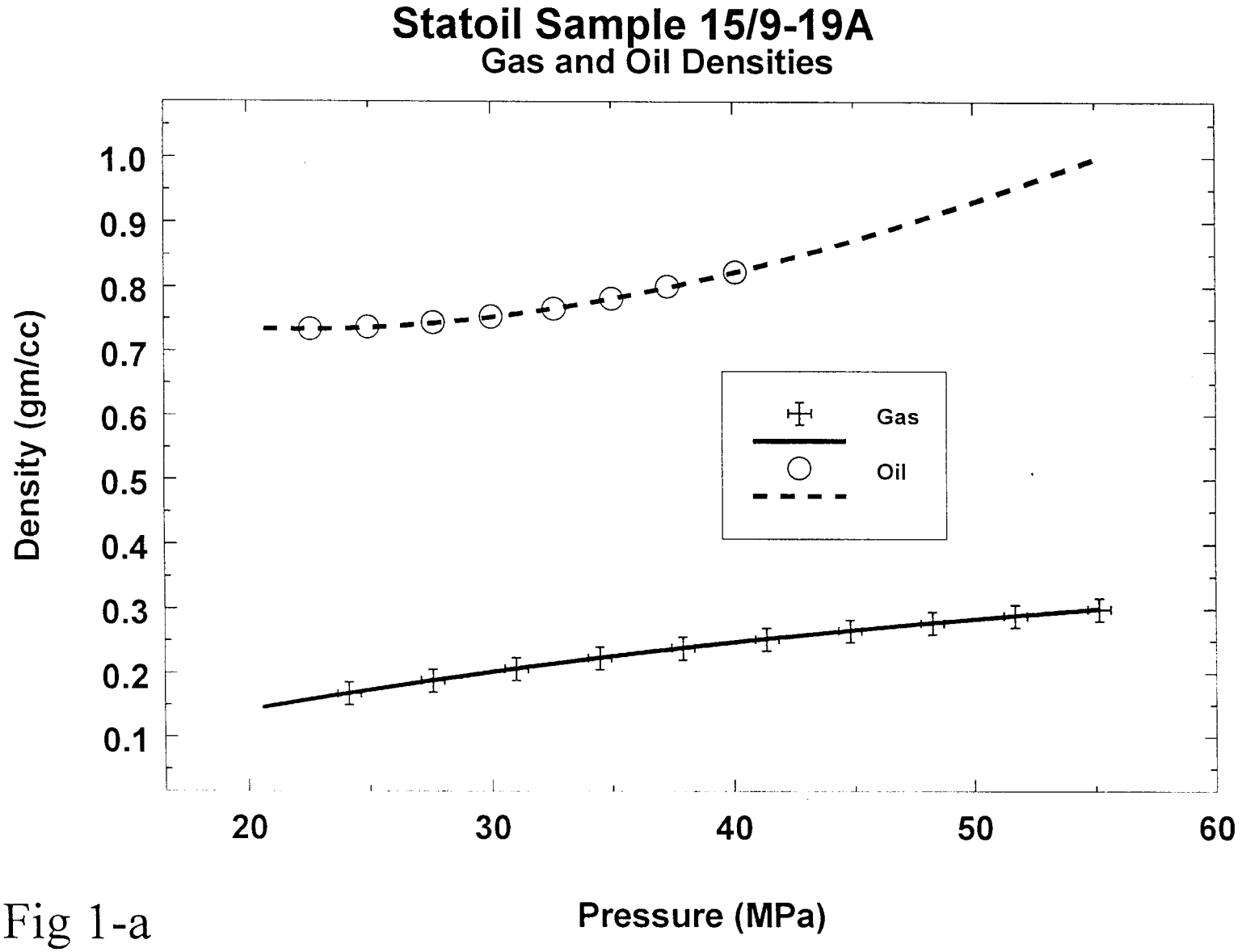
Statoil Sample 15/9-19A
Gas and Oil Densities
Density (gm/cc)
1.0
0.9
0.8
0.7
0.6
0.5
0.4
0.3
0.2
0.1
20
30
40
50
60
Pressure (MPa)
Gas
Oil

Fig 1-a

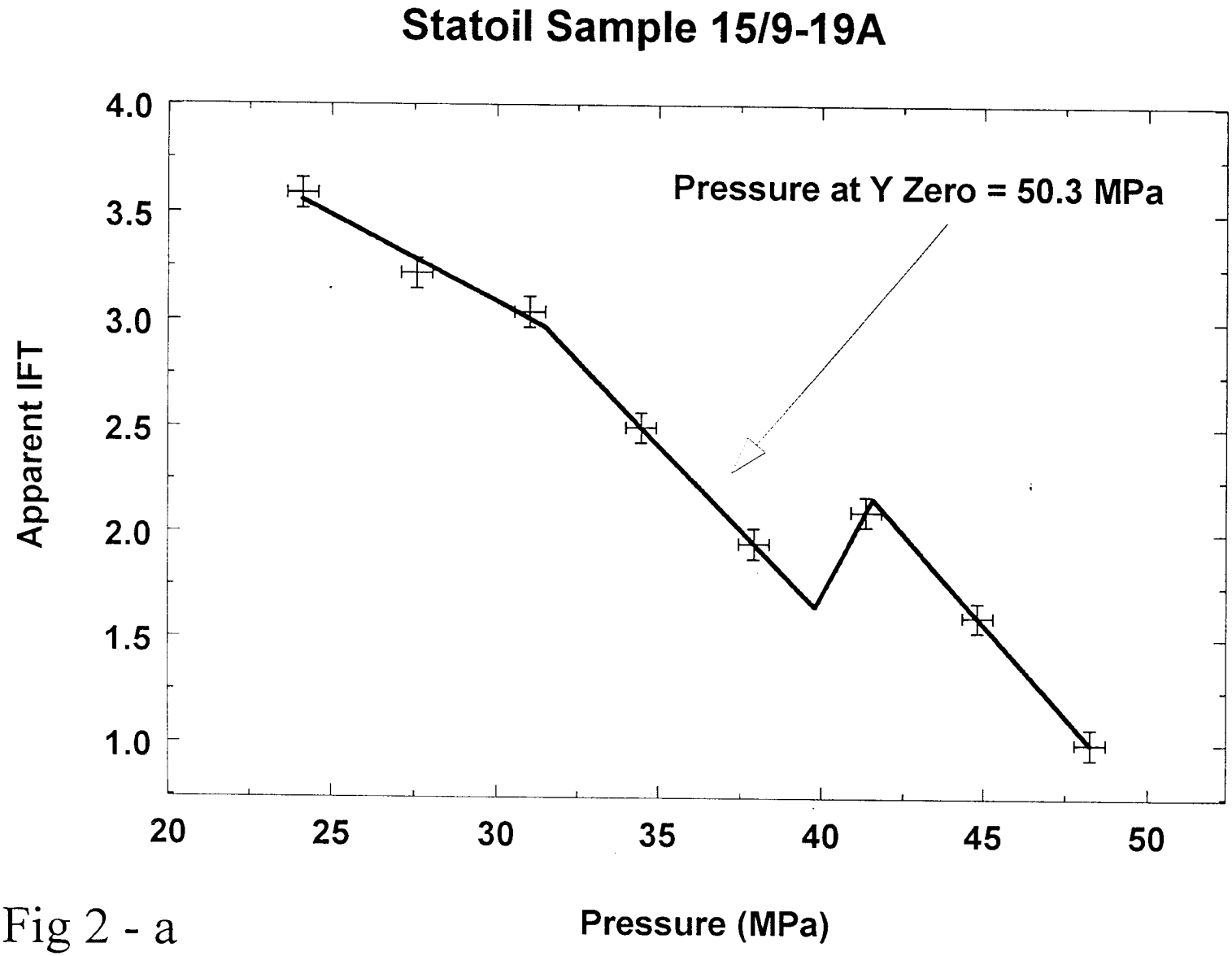
Statoil Sample 15/9-19A
Pressure at Y Zero = 50.3 MPa
Apparent IFT
4.0
3.5
3.0
2.5
2.0
1.5
1.0
20
25
30
35
40
45
50
Pressure (MPa)

Fig 2 - a

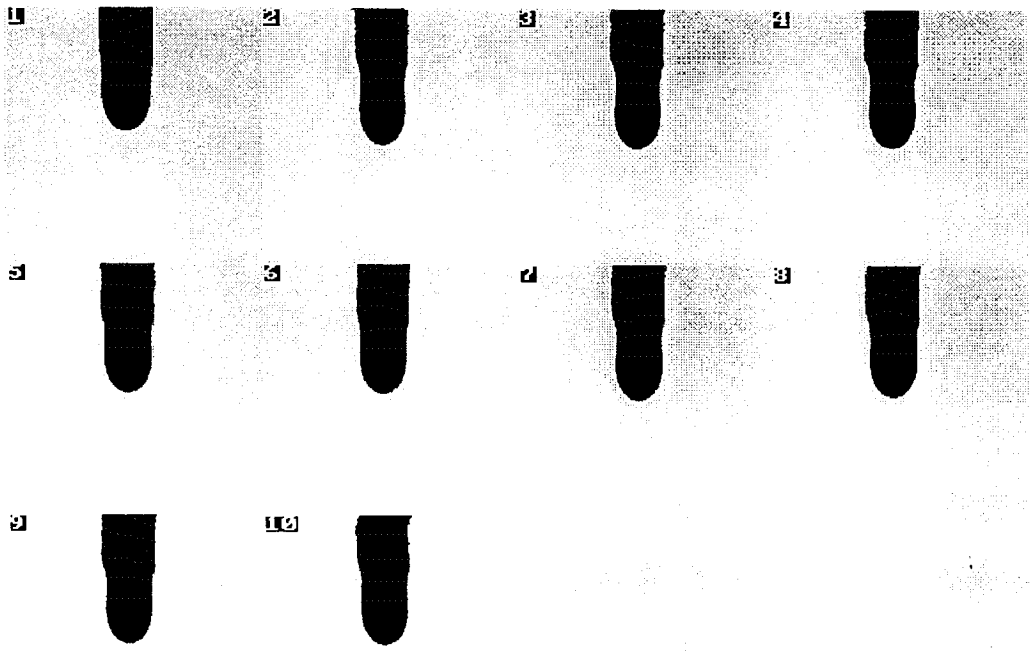
1
2
3
4
5
6
7
8
9
10
Statoil Sample 15/9-19A
Mixed Gas at 24.1 MPa and 110 C

Fig 3 - a

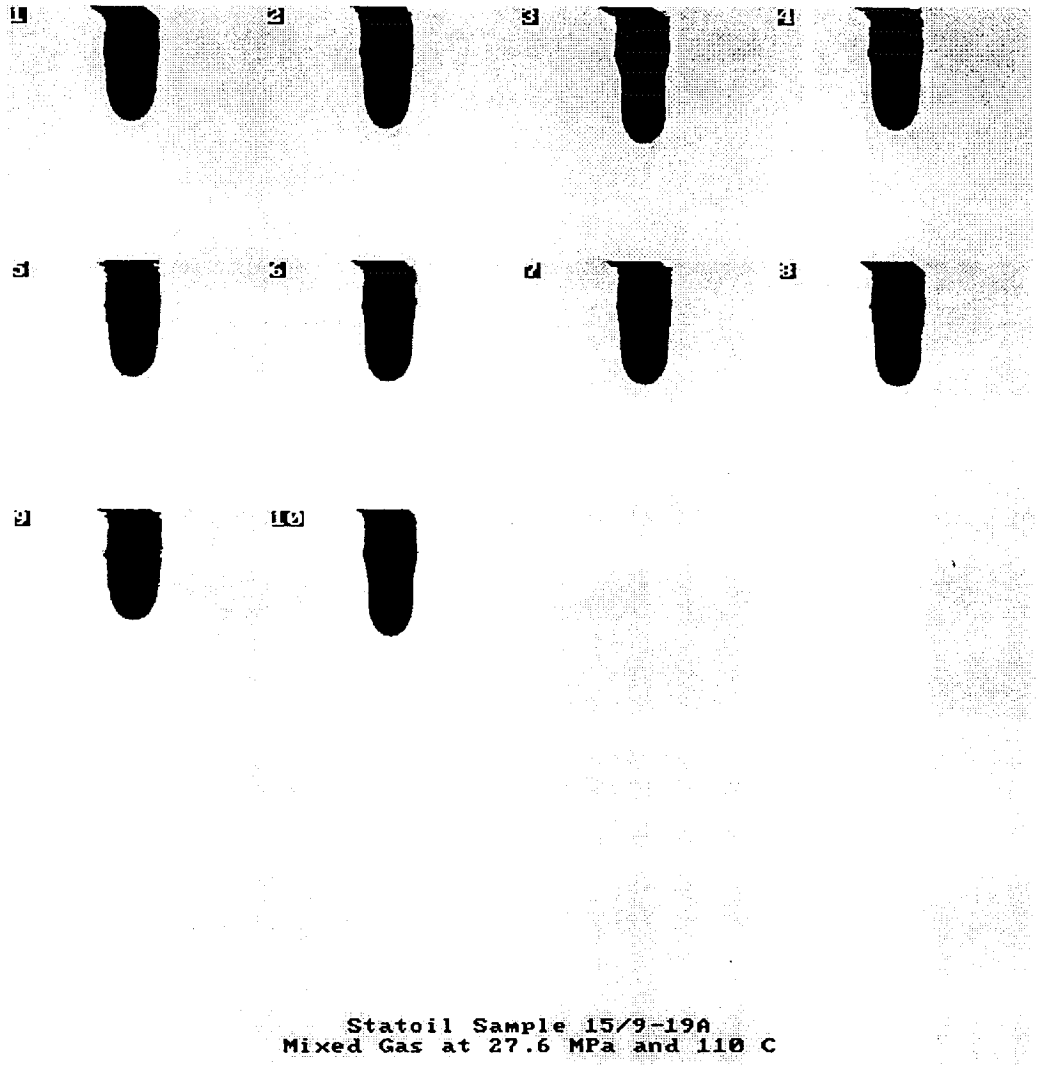
1
2
3
4
5
6
7
8
9
10
Statoil Sample 15/9-19A
Mixed Gas at 27.6 MPa and 110 C

Fig 4 - a

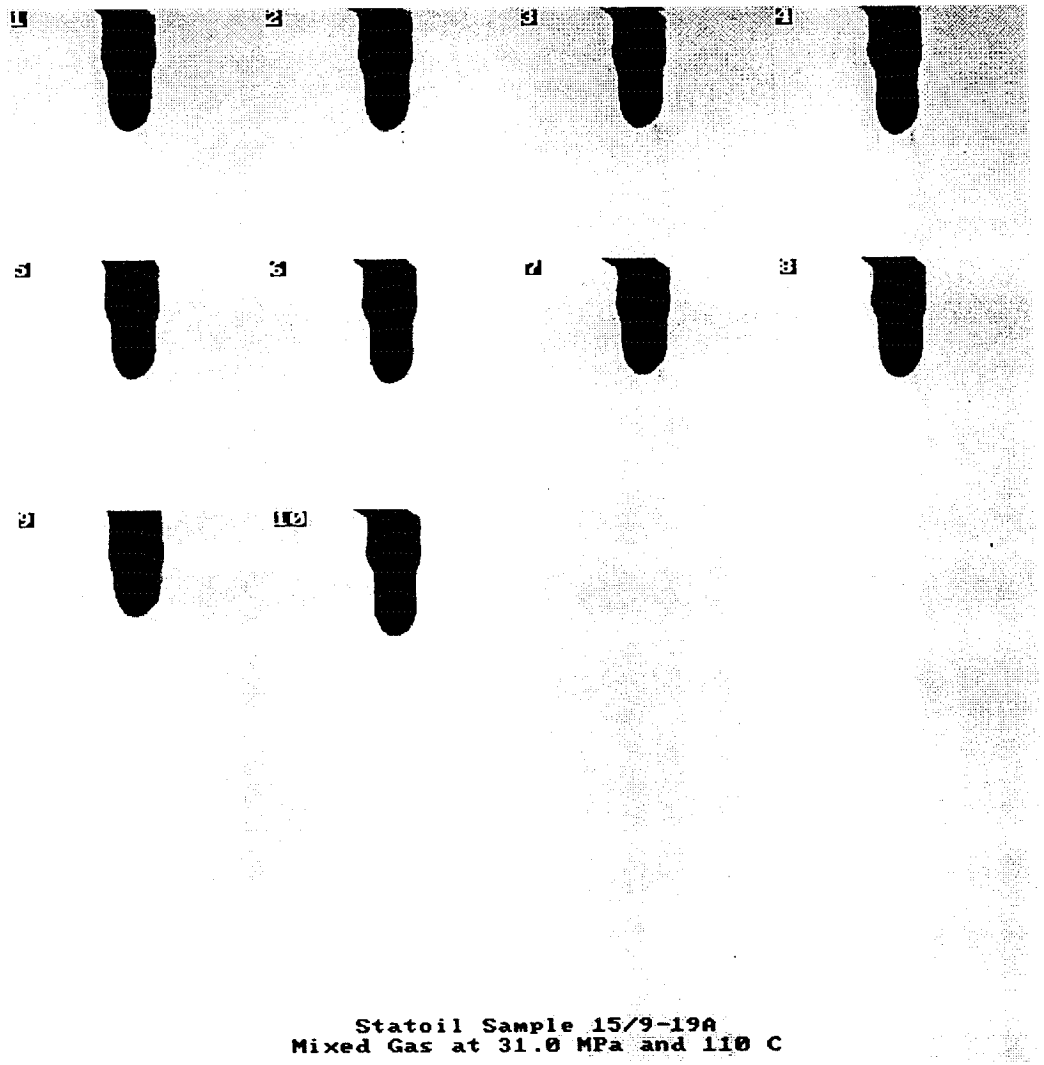
1
2
3
4
5
6
7
8
9
10
Statoil Sample 15/9-19A
Mixed Gas at 31.0 MPa and 110 C

Fig 5 - a

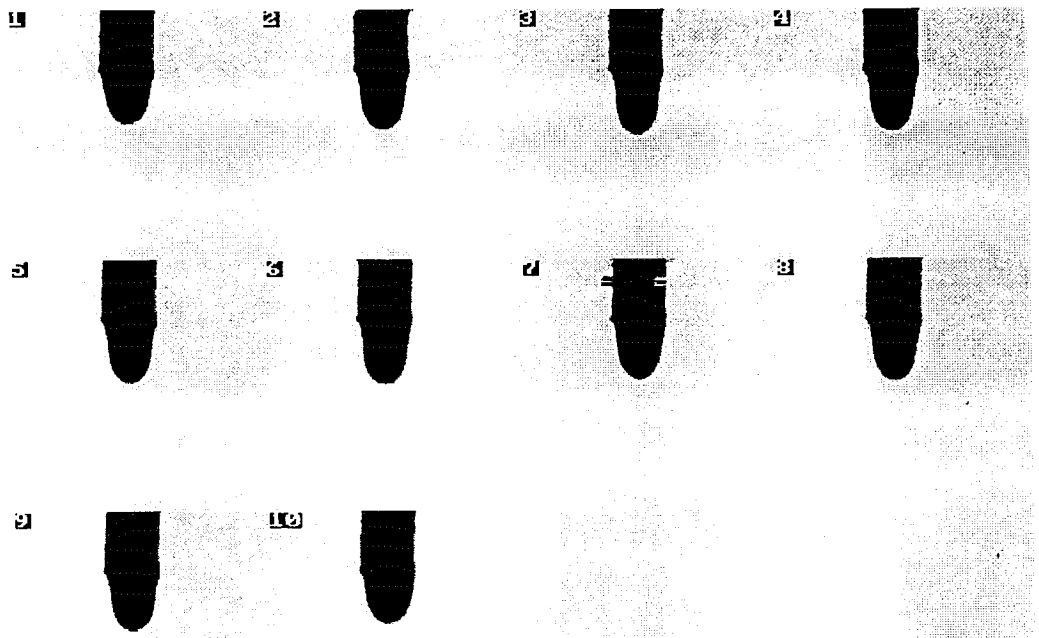

Statoil Sample 15/9-19A
Mixed Gas at 34.5 MPa and 110 C

Fig 6 - a

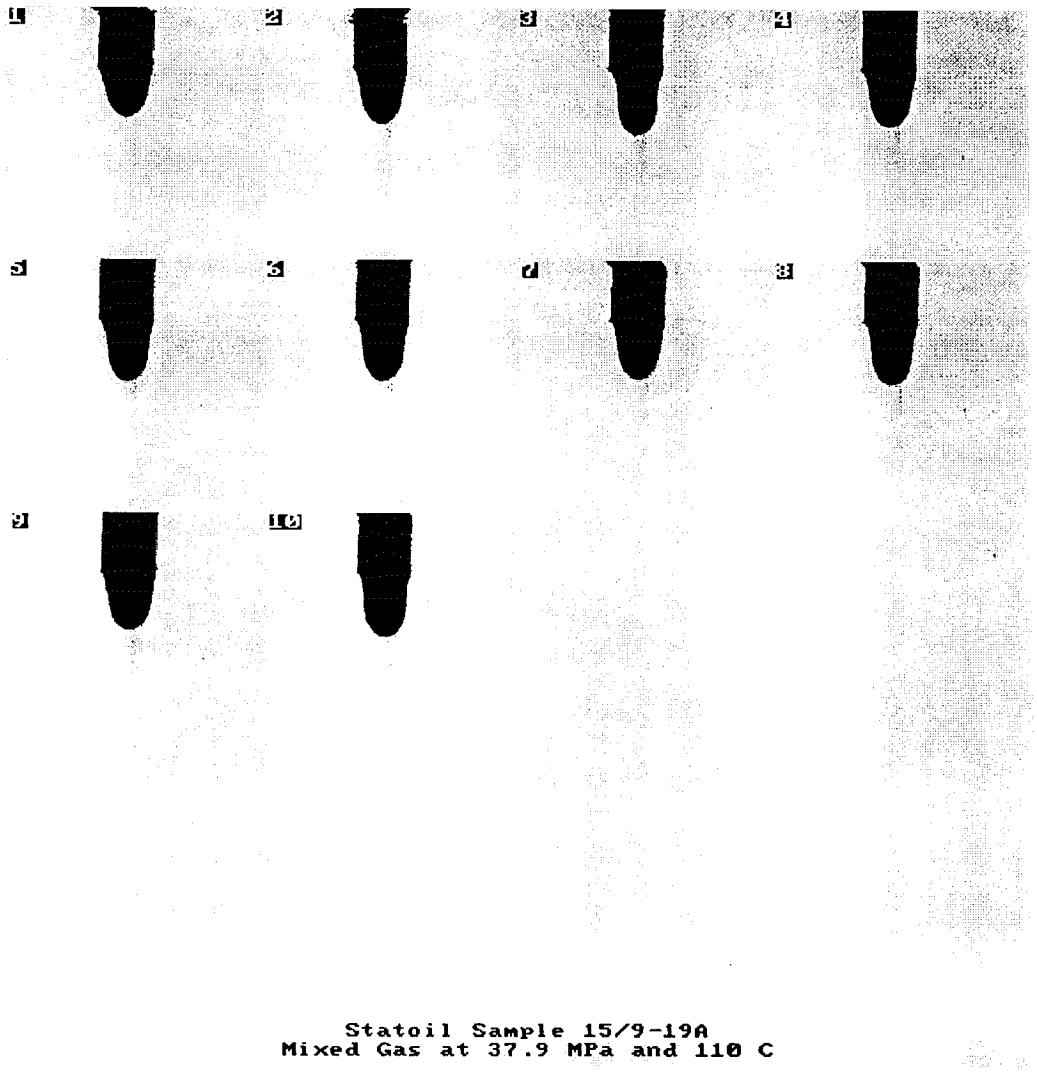

Fig 7 - a

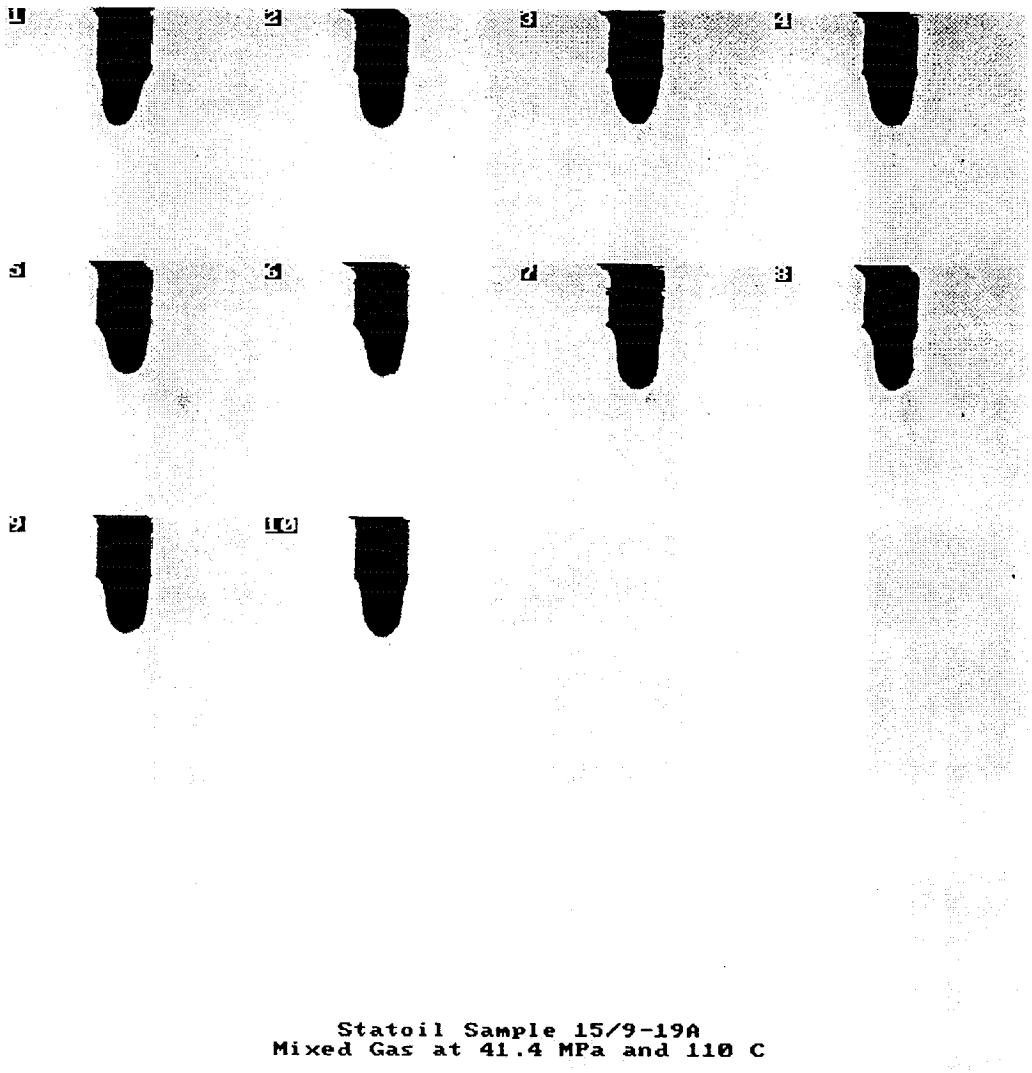

Fig 8 - a

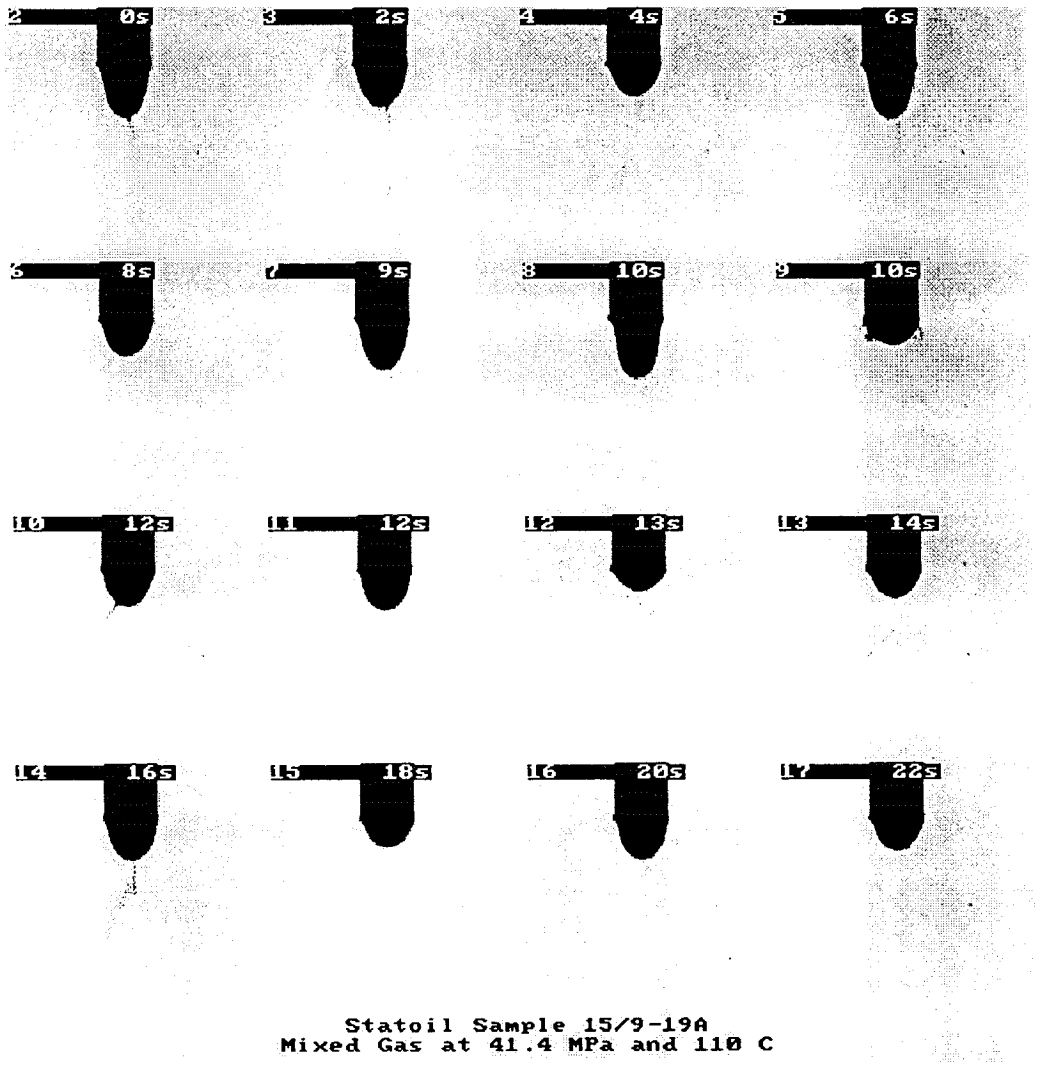
2 0s
3 2s
4 4s
5 6s
6 8s
7 9s
8 10s
9 10s
10 12s
11 12s
12 13s
13 14s
14 16s
15 18s
16 20s
17 22s
Statoil Sample 15/9-19A
Mixed Gas at 41.4 MPa and 110 C

Fig 9 - a

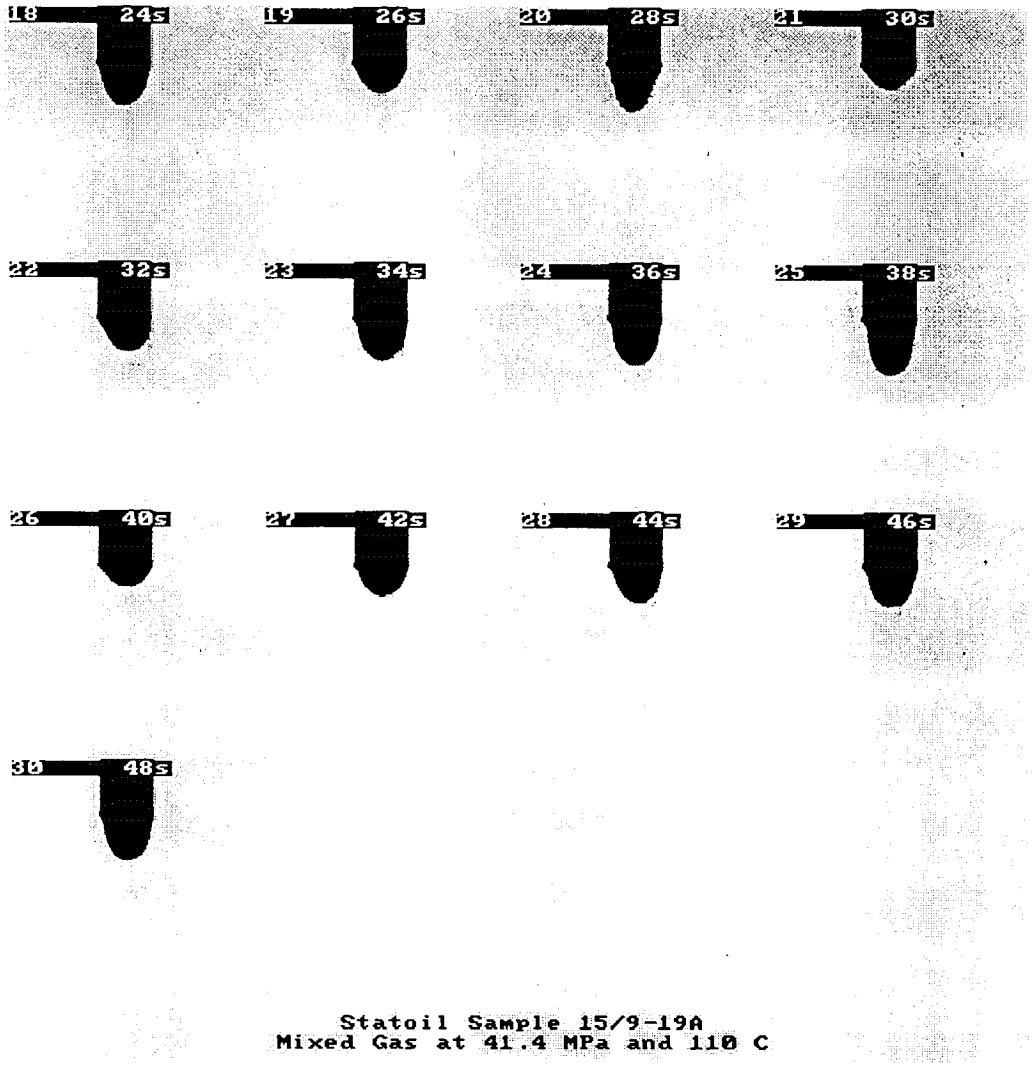
18 24s
19 26s
20 28s
21 30s
22 32s
23 34s
24 36s
25 38s
26 40s
27 42s
28 44s
29 46s
30 48s
Statoil Sample 15/9-19A
Mixed Gas at 41.4 MPa and 110 C

Fig 10 - a

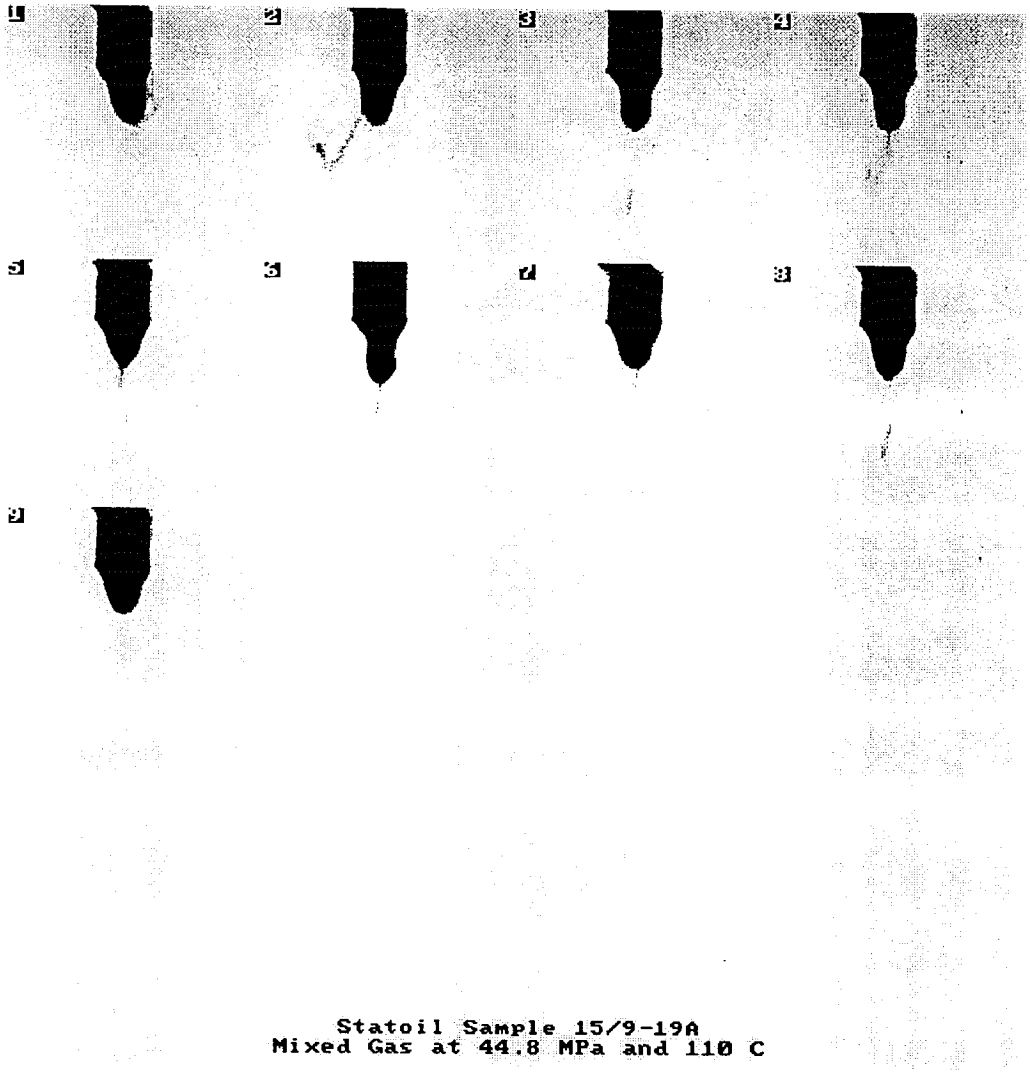
1
2
3
4
5
6
7
8
9
Statoil Sample 15/9-19A
Mixed Gas at 44.8 MPa and 110 C

Fig 11 - a

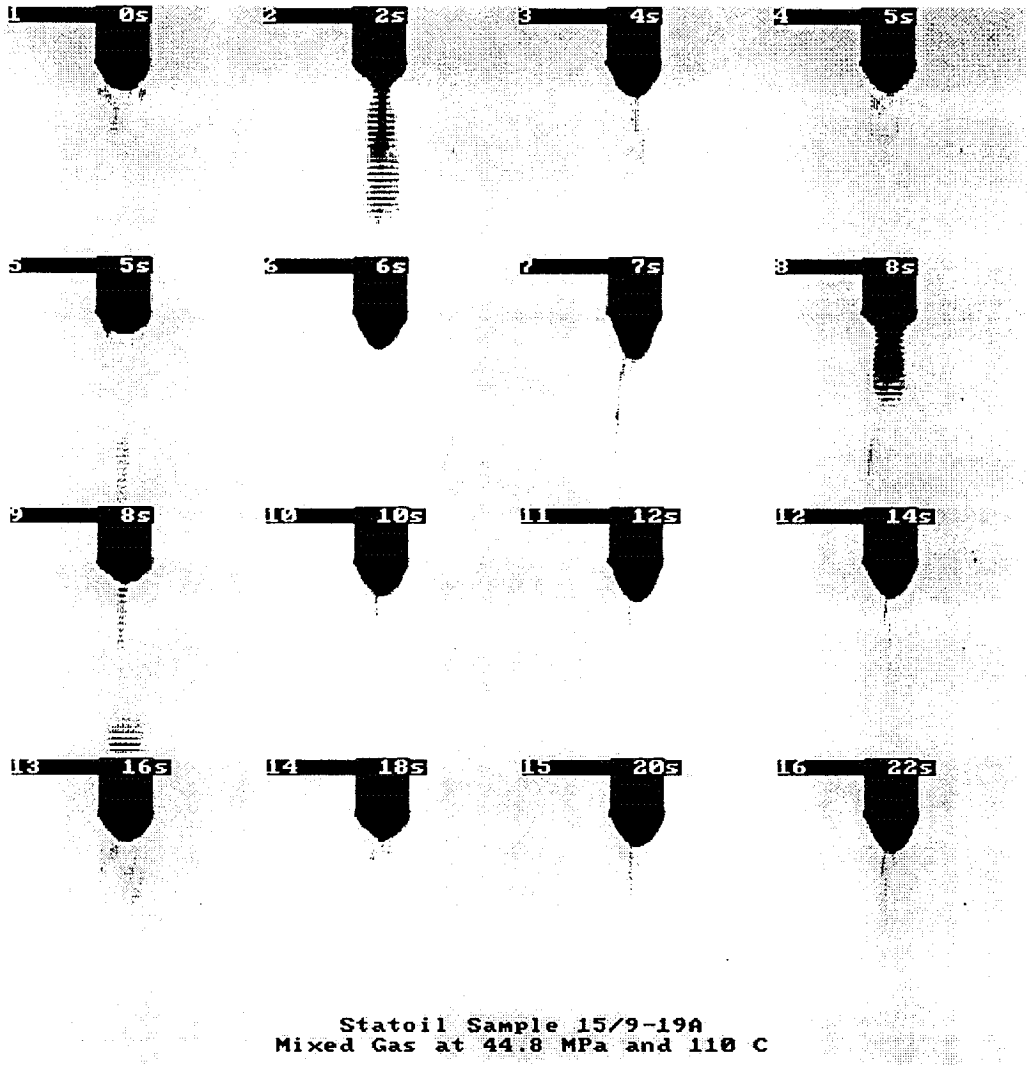
1 0s
2 2s
3 4s
4 5s
5 5s
6 6s
7 7s
8 8s
9 8s
10 10s
11 12s
12 14s
13 16s
14 18s
15 20s
16 22s
Statoil Sample 15/9-19A
Mixed Gas at 44.8 MPa and 110 C

Fig 12 - a

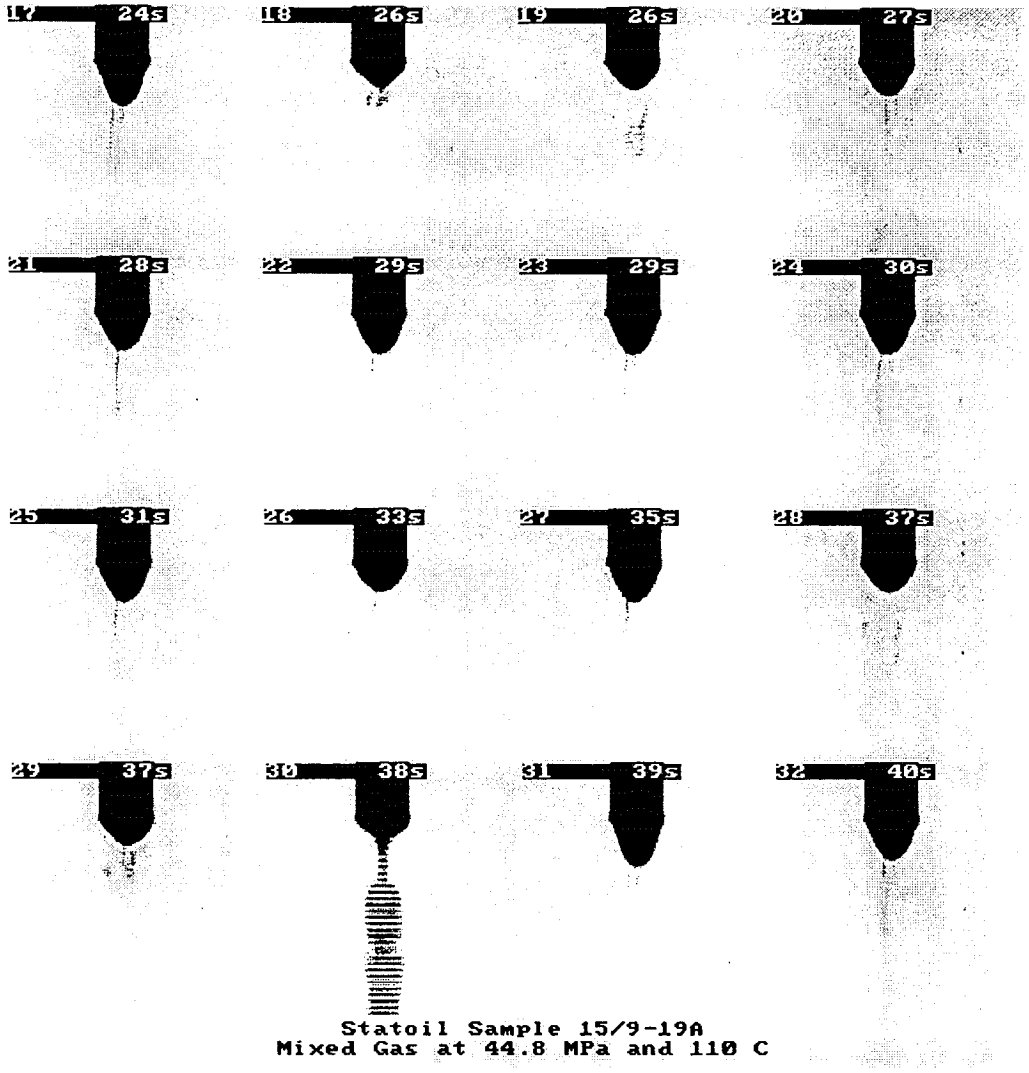
17 24s
18 26s
19 26s
20 27s
21 28s
22 29s
23 29s
24 30s
25 31s
26 33s
27 35s
28 37s
29 37s
30 38s
31 39s
32 40s
Statoil Sample 15/9-19A
Mixed Gas at 44.8 MPa and 110 C

Fig 13 - a

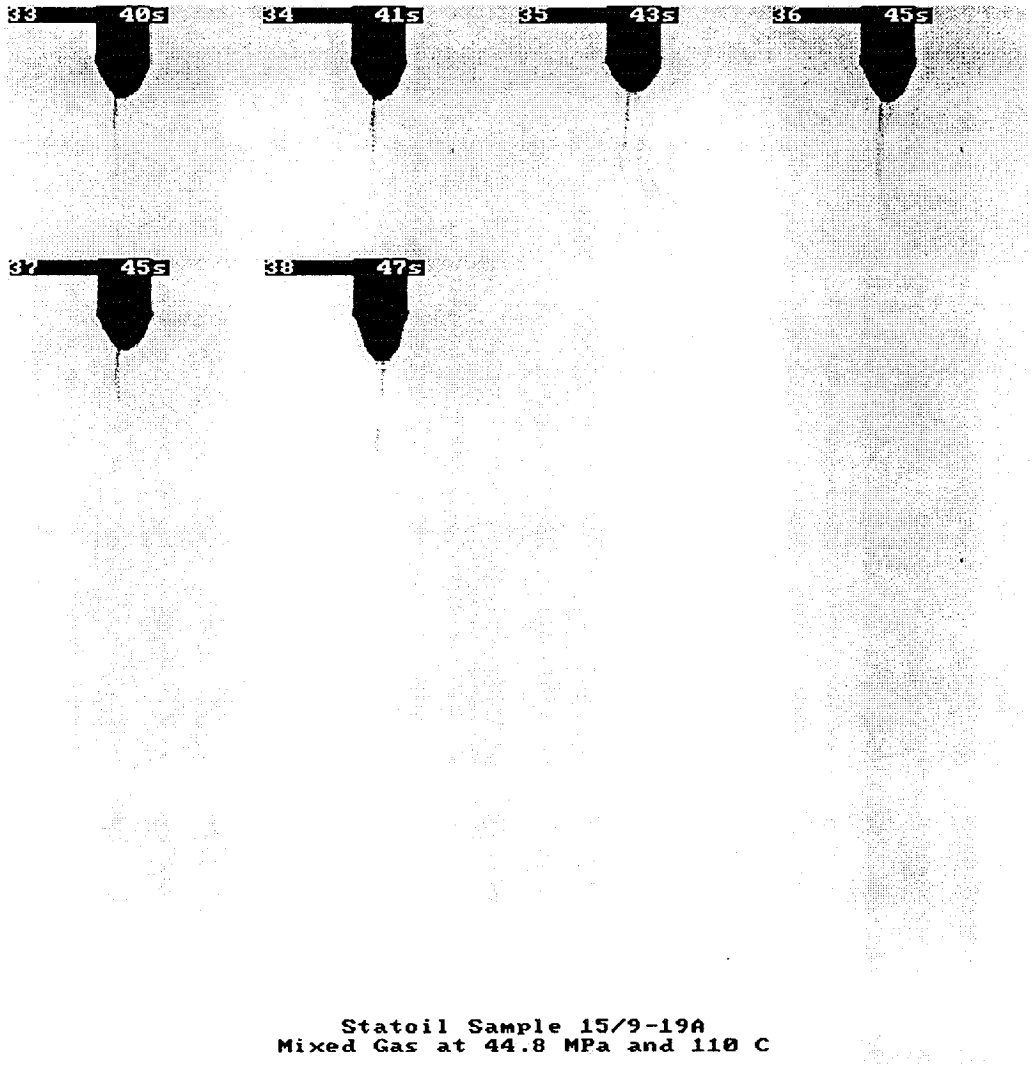
33 40s
34 41s
35 43s
36 45s
37 45s
38 47s
Statoil Sample 15/9-19A
Mixed Gas at 44.8 MPa and 110 C

Fig 14 - a

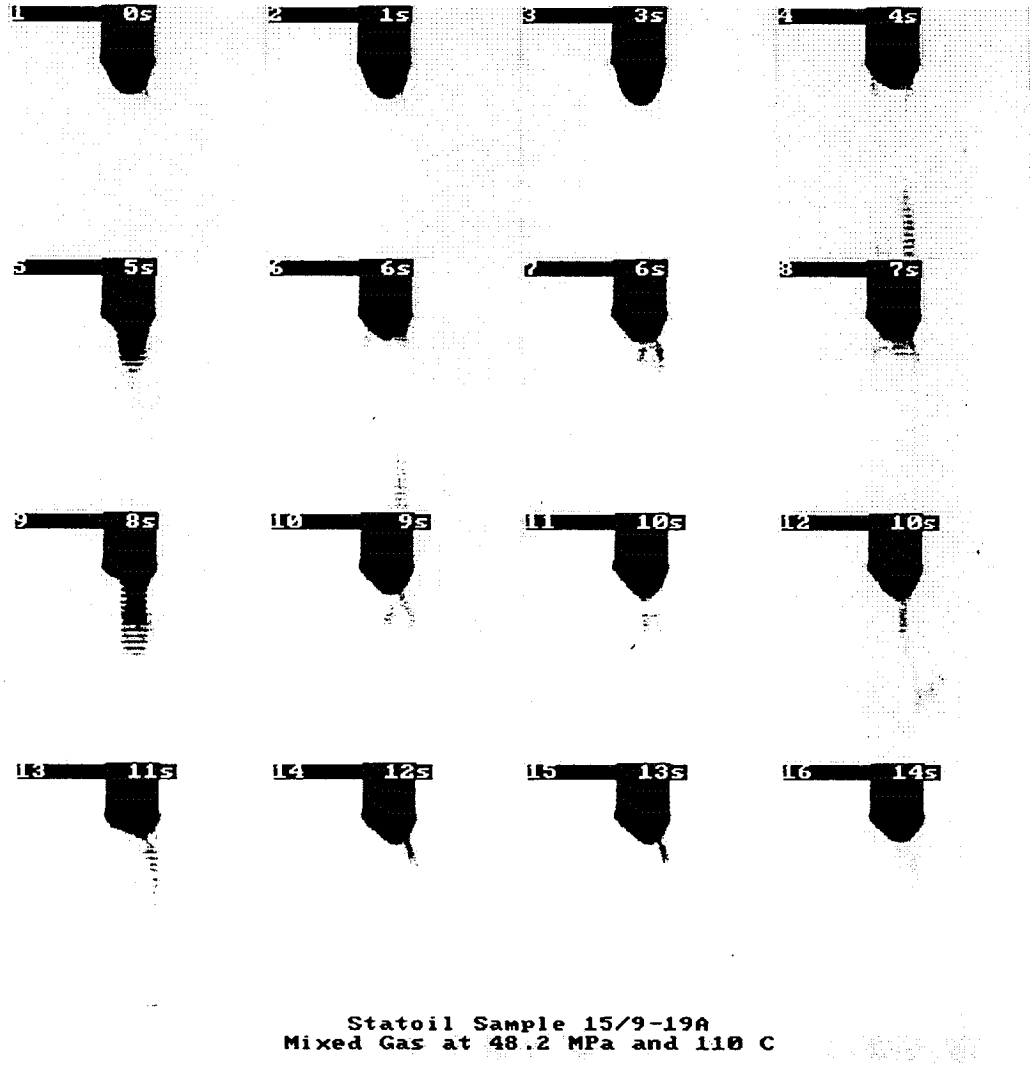
1 0s
2 1s
3 3s
4 4s
5 5s
6 6s
7 6s
8 7s
9 8s
10 9s
11 10s
12 10s
13 11s
14 12s
15 13s
16 14s
Statoil Sample 15/9-19A
Mixed Gas at 48.2 MPa and 110 C

Fig 15 - a

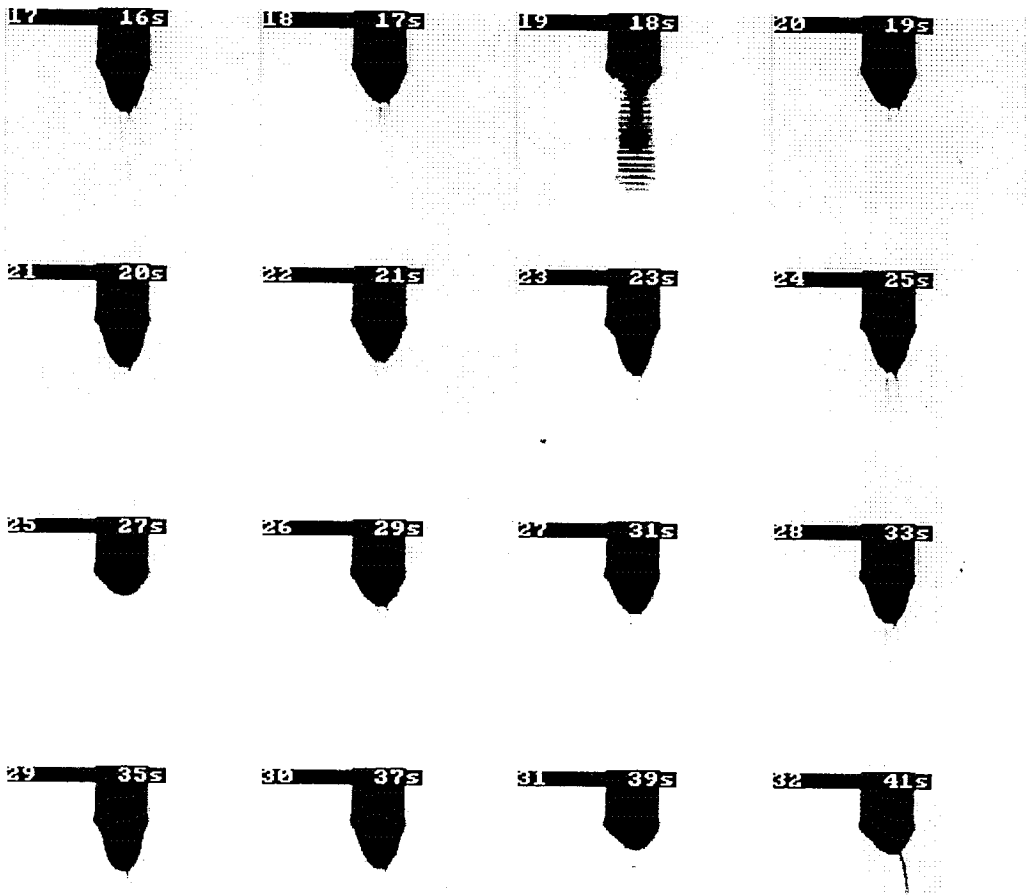

Statoil Sample 15/9-19A
Mixed Gas at 48.2 MPa and 110 C

Fig 16 - a

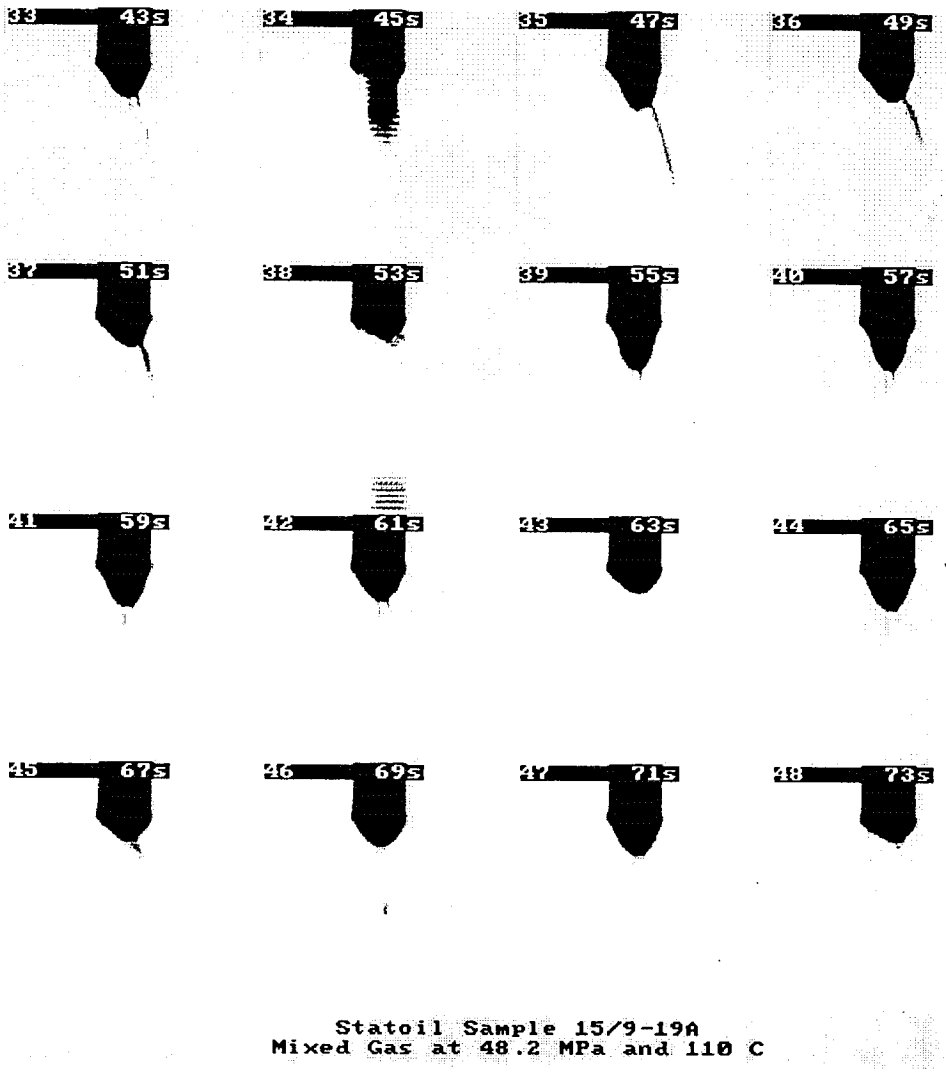
33 43s
34 45s
35 47s
36 49s
37 51s
38 53s
39 55s
40 57s
41 59s
42 61s
43 63s
44 65s
45 67s
46 69s
47 71s
48 73s
Statoil Sample 15/9-19A
Mixed Gas at 48.2 MPa and 110 C

Fig 17 - a

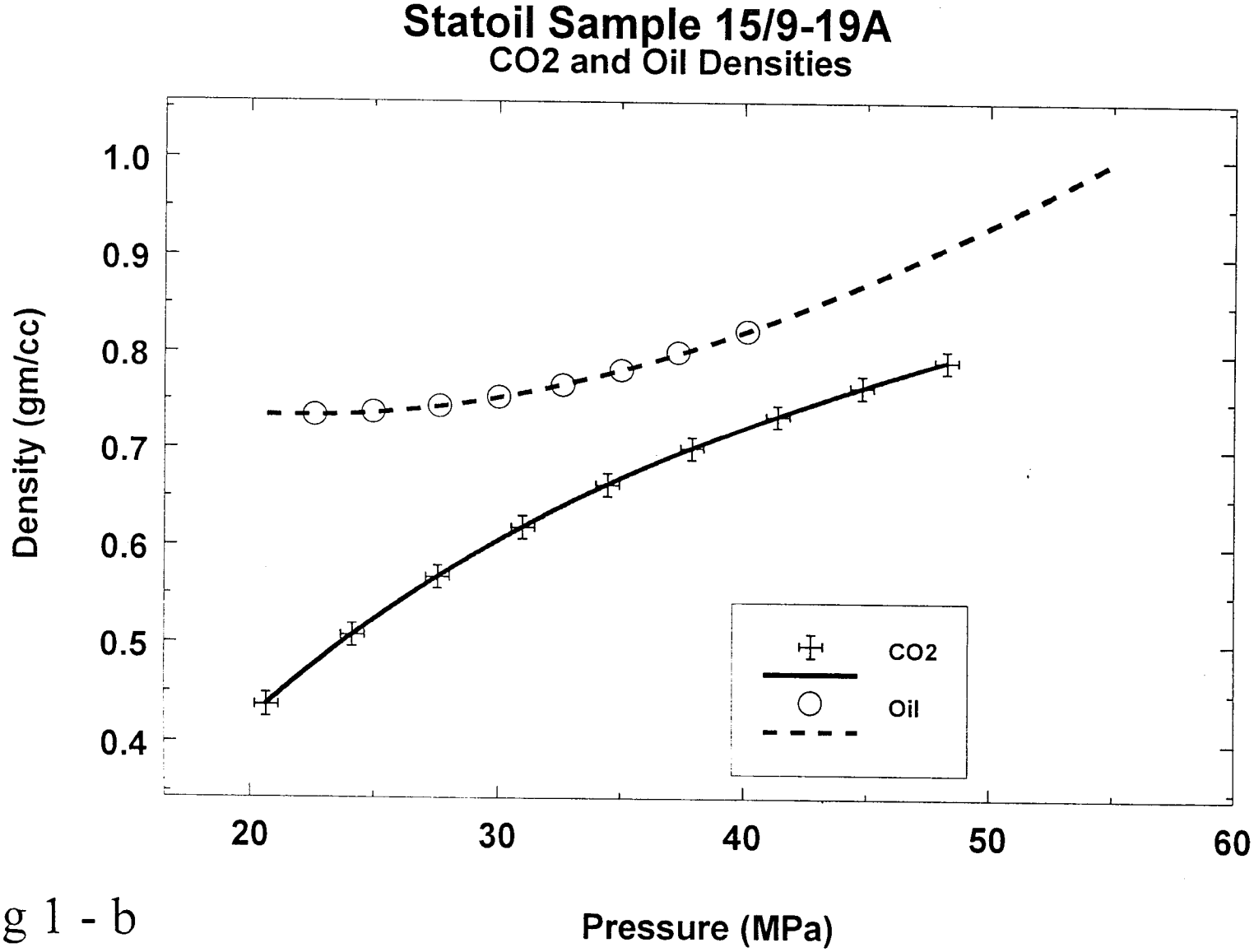
Statoil Sample 15/9-19A
CO2 and Oil Densities
Density (gm/cc)
1.0
0.9
0.8
0.7
0.6
0.5
0.4
20
30
40
50
60
Pressure (MPa)
CO2
Oil

Fig 1 - b

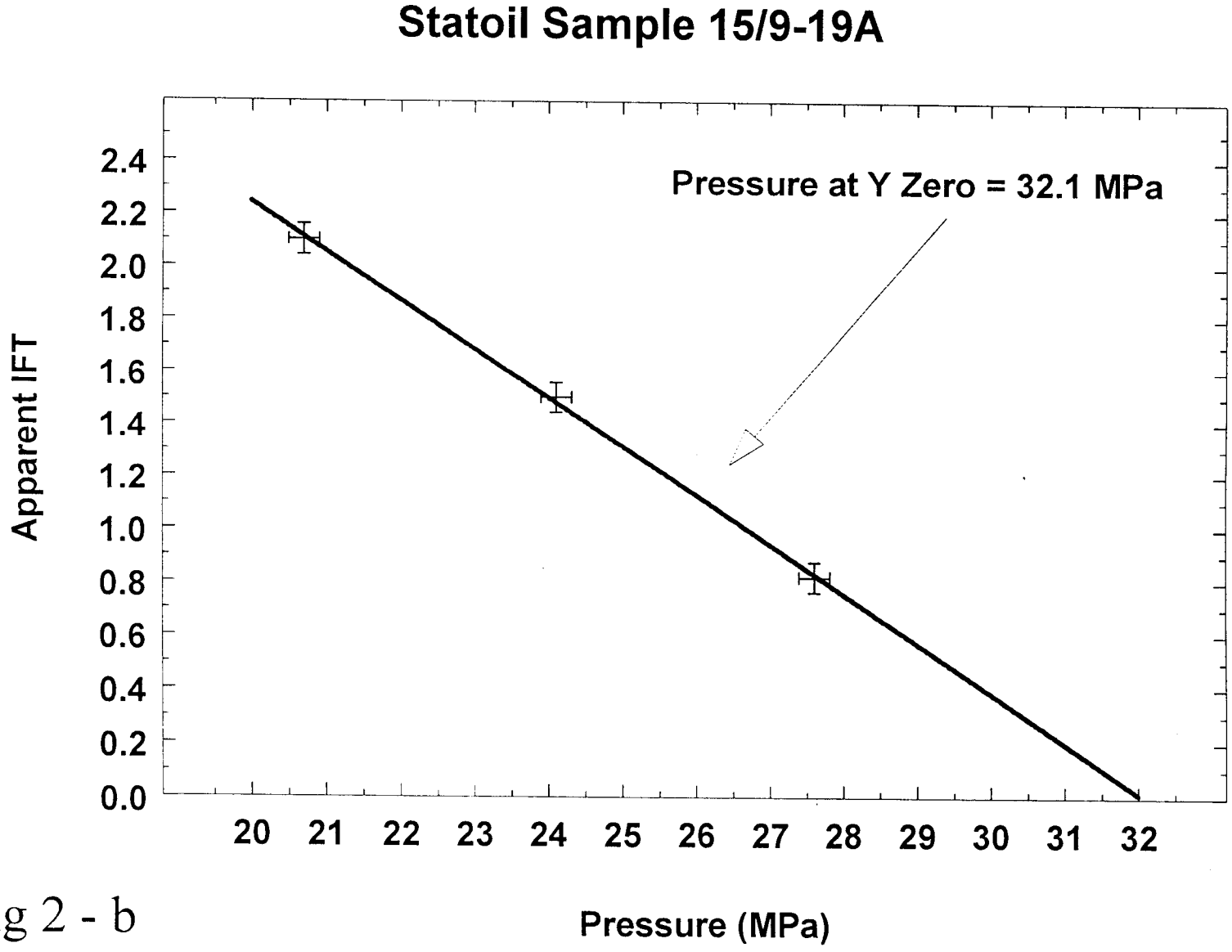
Statoil Sample 15/9-19A
Pressure at Y Zero = 32.1 MPa
Apparent IFT
2.4
2.2
2.0
1.8
1.6
1.4
1.2
1.0
0.8
0.6
0.4
0.2
0.0
20
21
22
23
24
25
26
27
28
29
30
31
32
Pressure (MPa)

Fig 2 - b

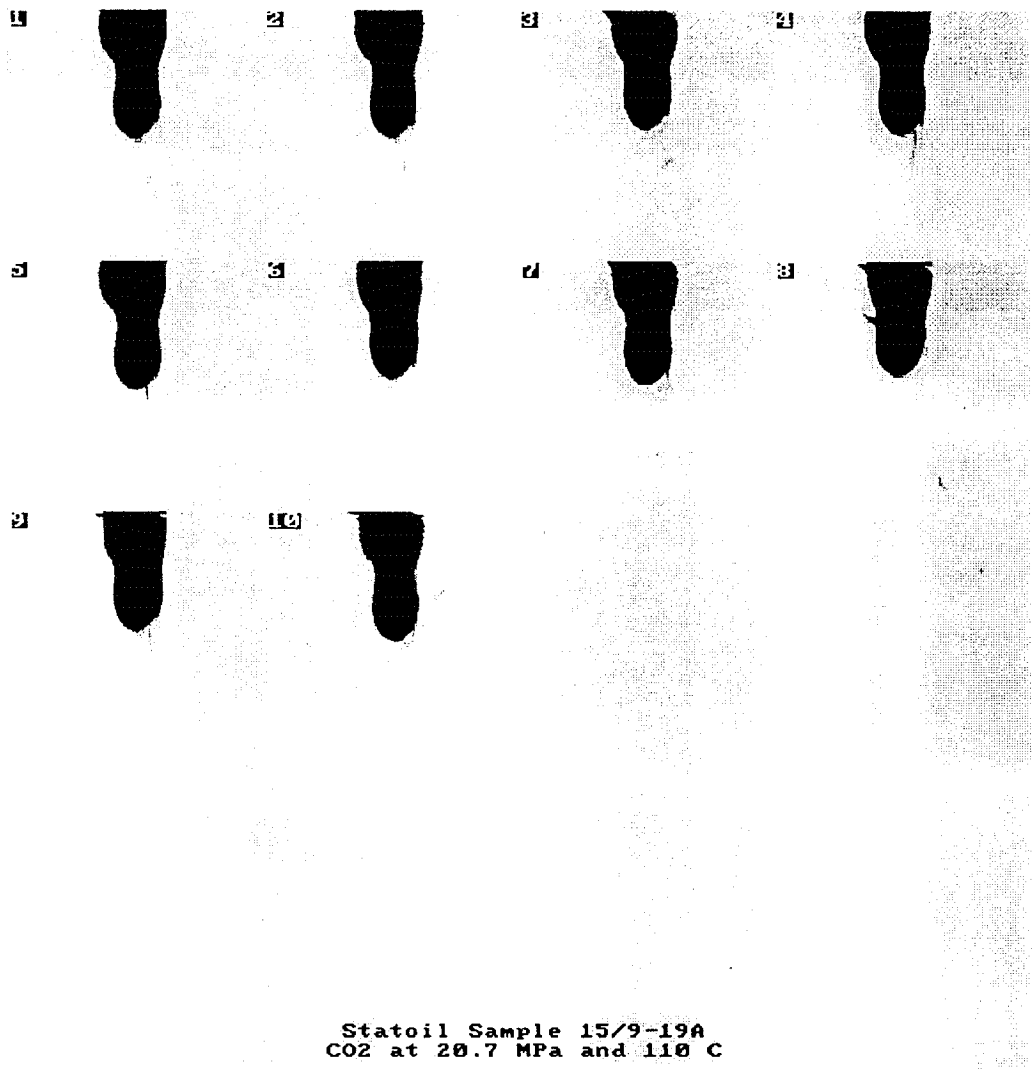

Fig 3 - b

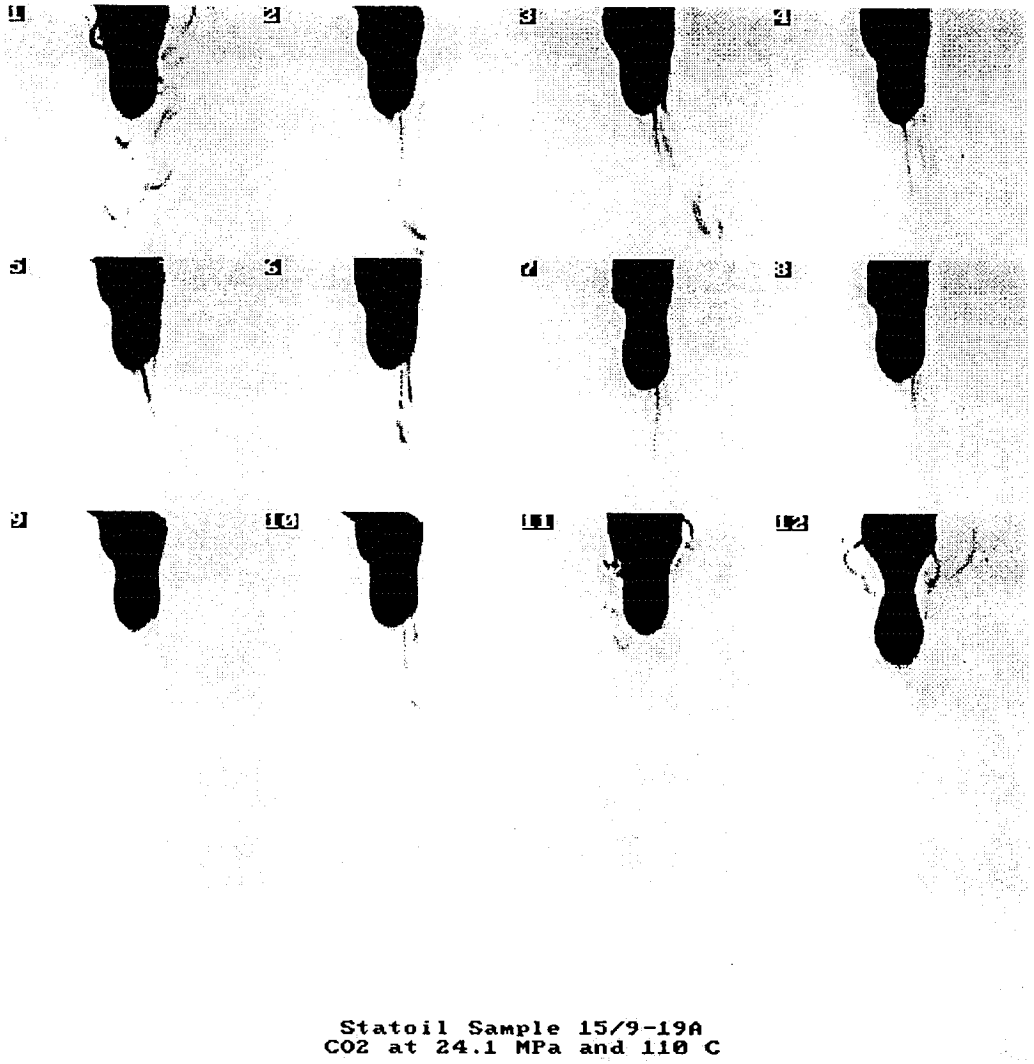

Statoil Sample 15/9-19A
CO2 at 24.1 MPa and 110 C

Fig 4 - b

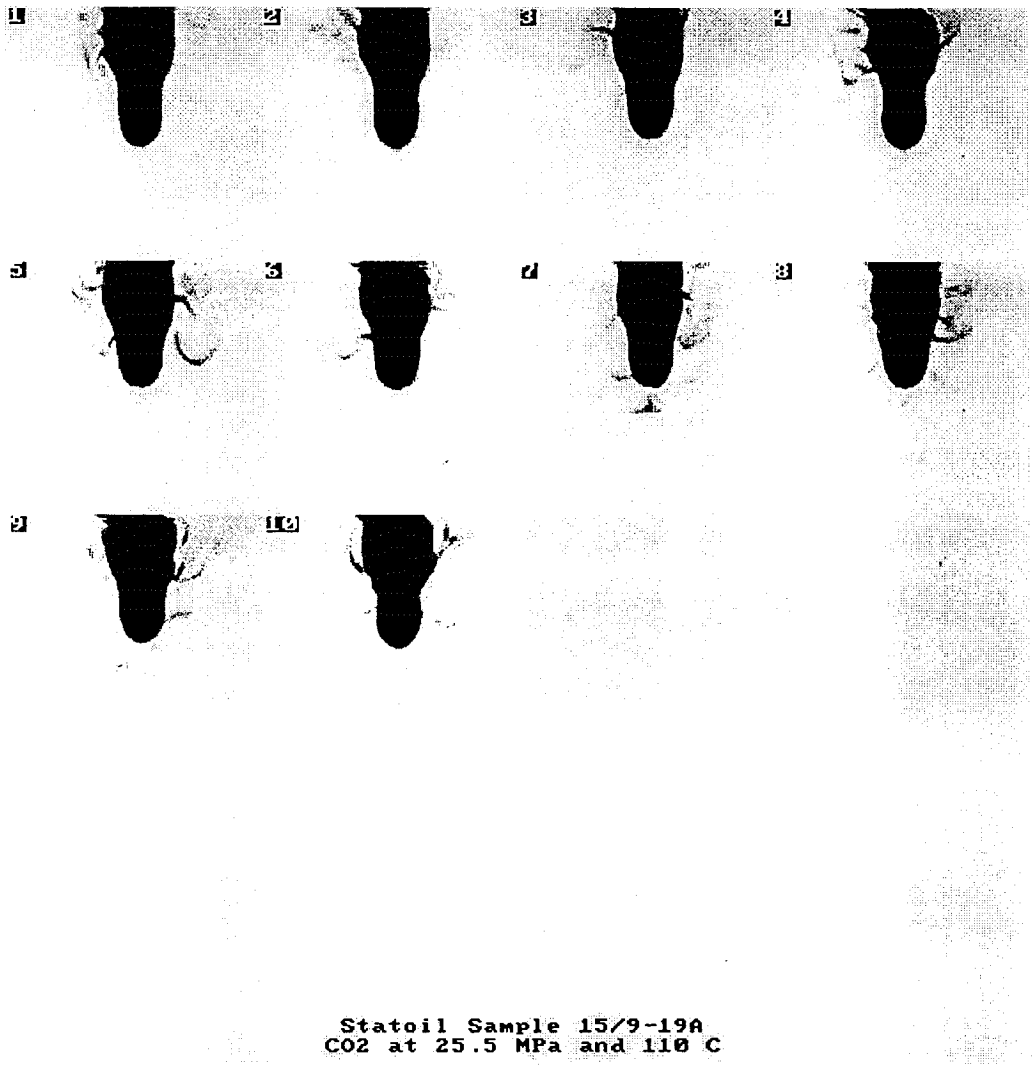

Fig 5 - b

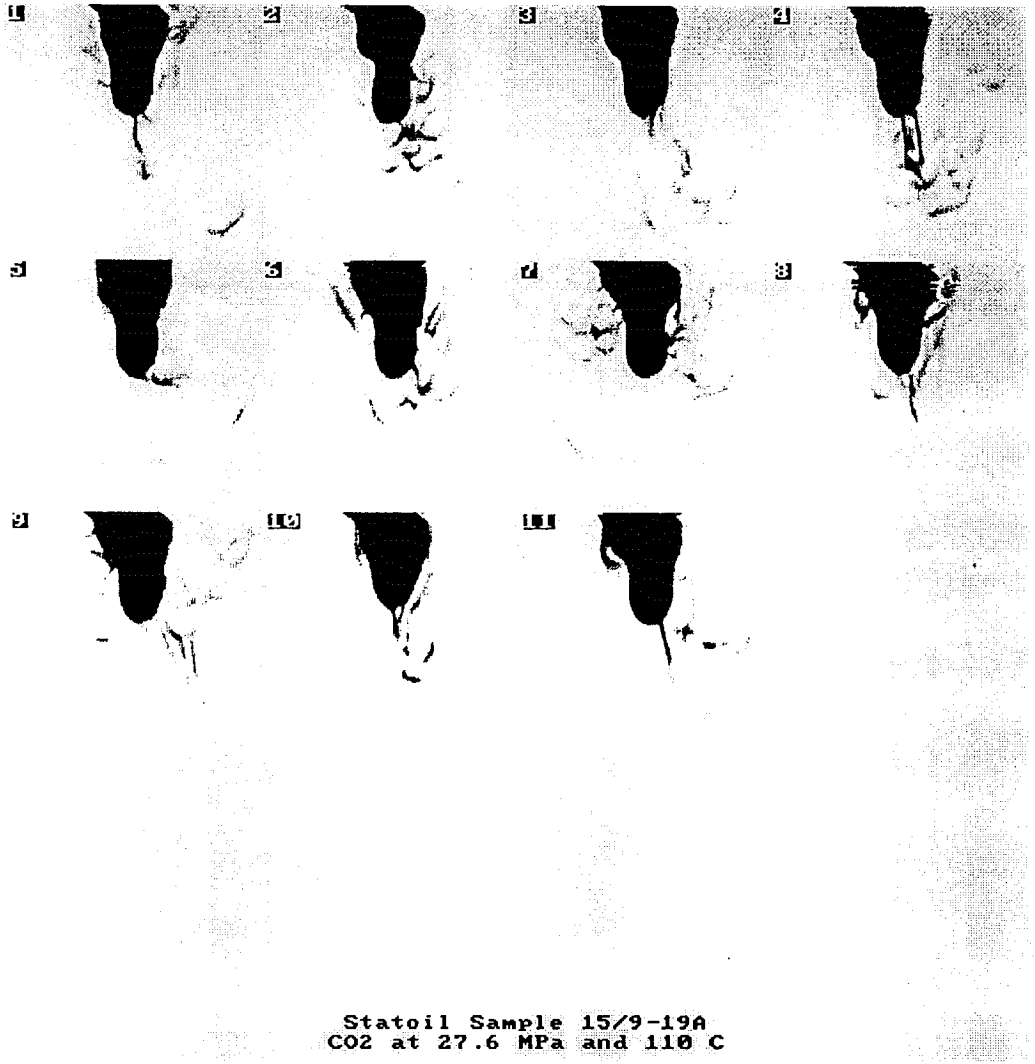

Fig 6 - b

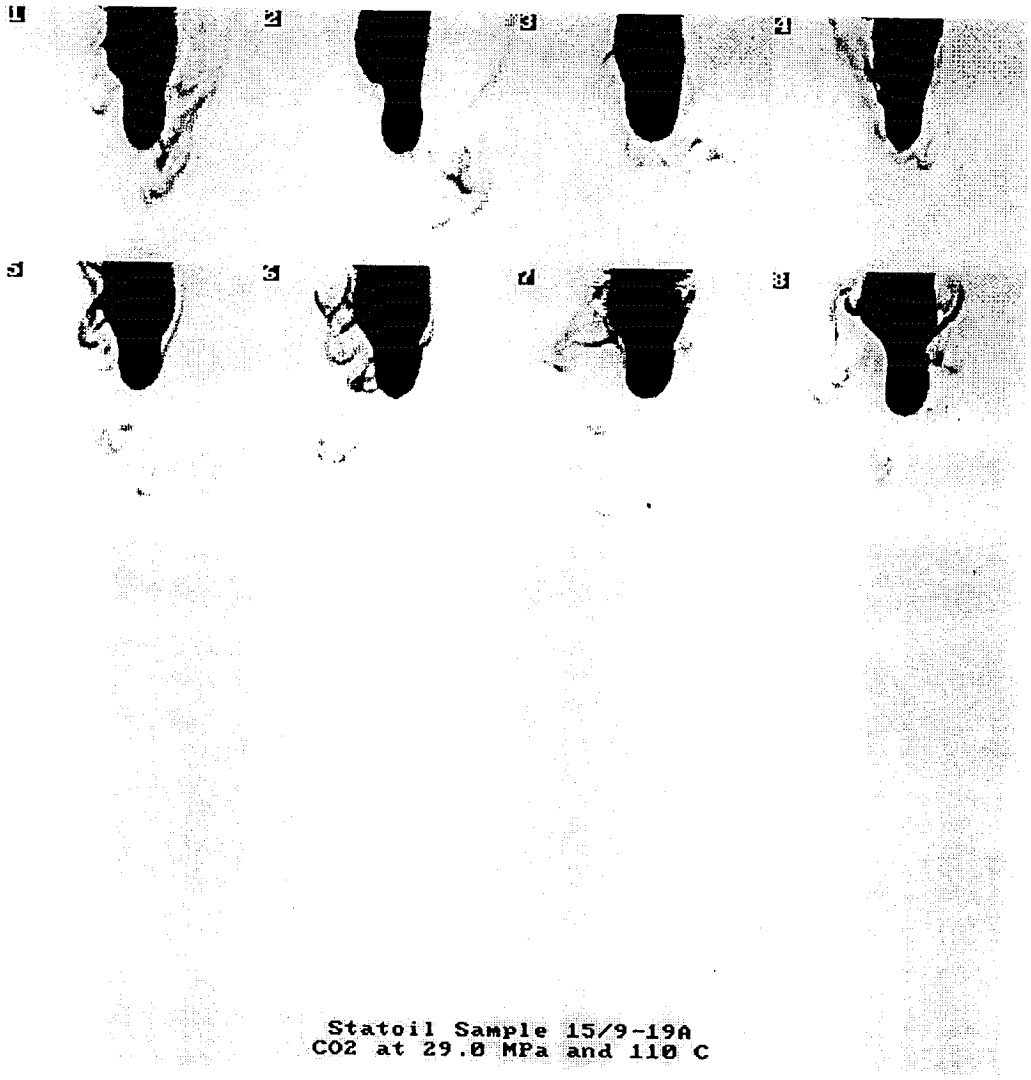

Fig 7 - b

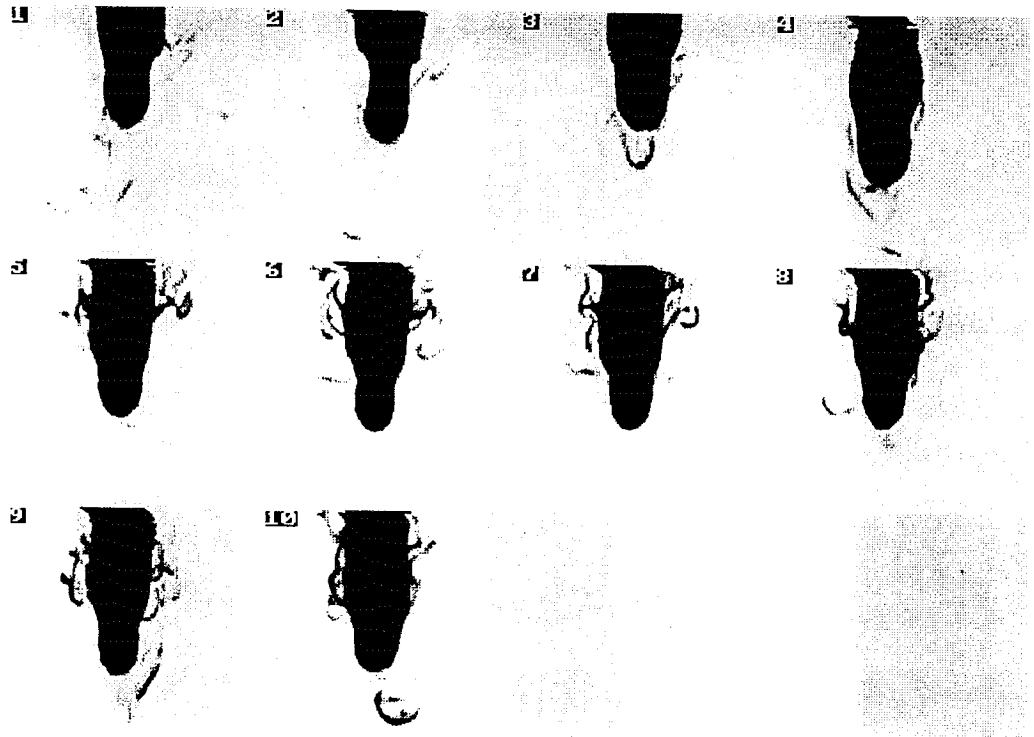

Statoil Sample 15/9-19A
CO2 at 31.0 MPa and 110 C

Fig 8 - b

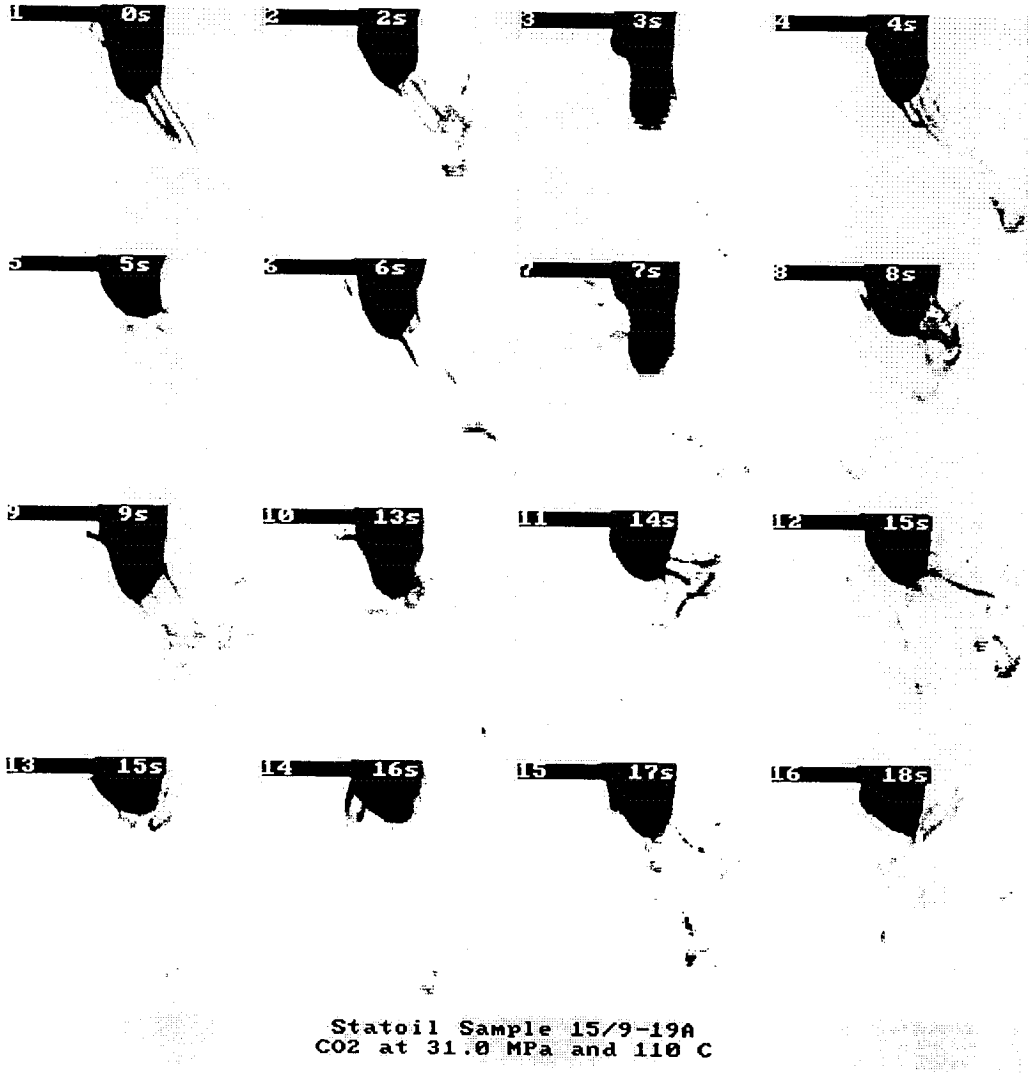
1 0s
2 2s
3 3s
4 4s
5 5s
6 6s
7 7s
8 8s
9 9s
10 13s
11 14s
12 15s
13 15s
14 16s
15 17s
16 18s
Statoil Sample 15/9-19A
CO2 at 31.0 MPa and 110 C

Fig 9 - b

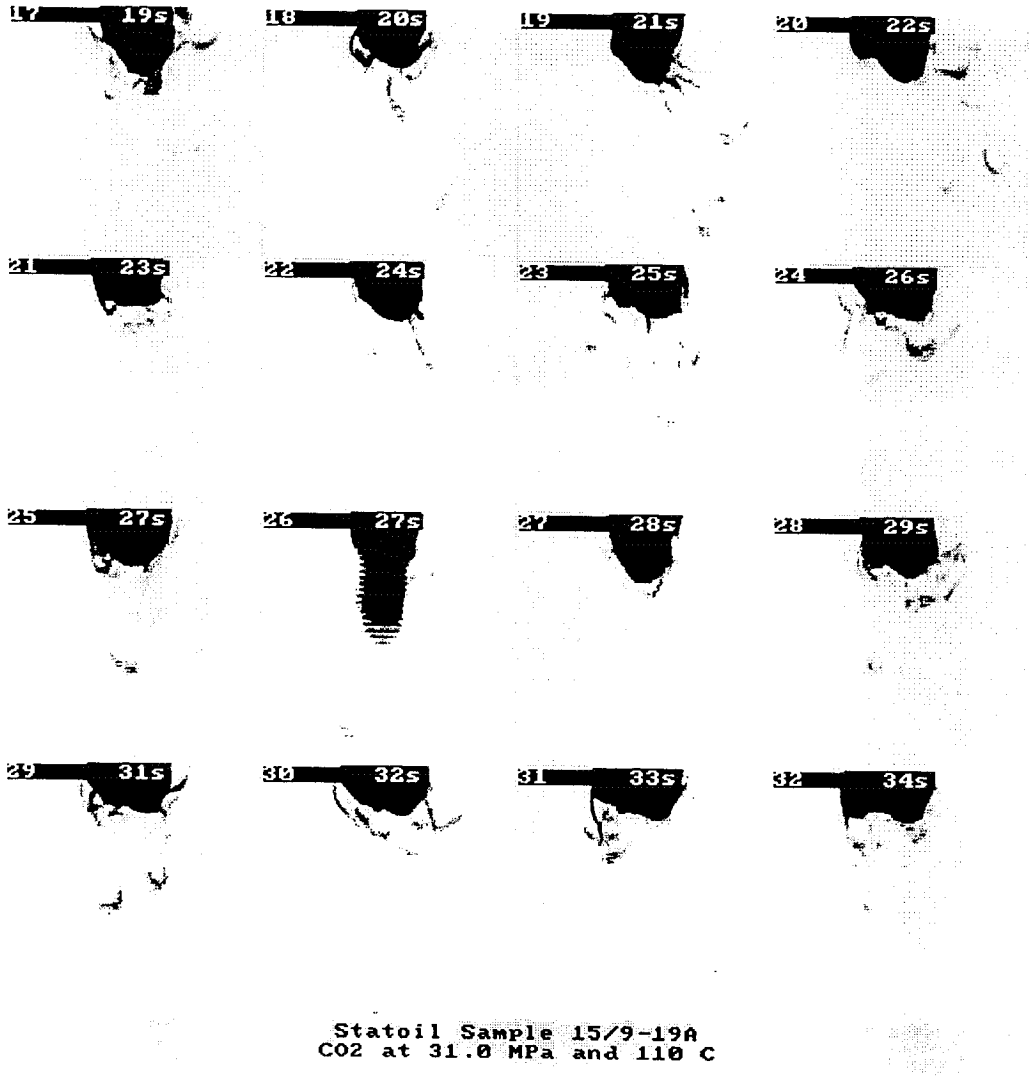
17 19s
18 20s
19 21s
20 22s
21 23s
22 24s
23 25s
24 26s
25 27s
26 27s
27 28s
28 29s
29 31s
30 32s
31 33s
32 34s
Statoil Sample 15/9-19A
CO2 at 31.0 MPa and 110 C

Fig 10 - b

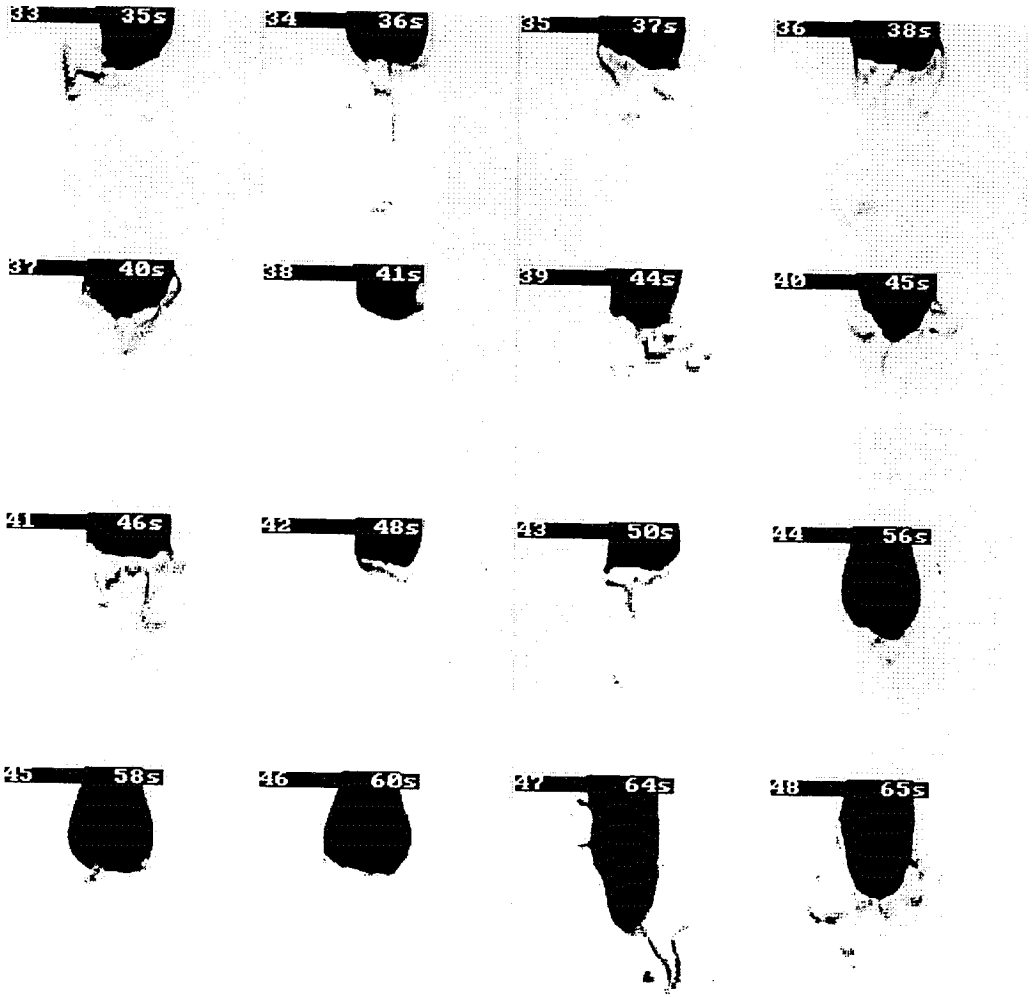
33 35s
34 36s
35 37s
36 38s
37 40s
38 41s
39 44s
40 45s
41 46s
42 48s
43 50s
44 56s
45 58s
46 60s
47 64s
48 65s
Statoil Sample 15/9-19A
CO2 at 31.0 MPa and 110 C

Fig 11 - b

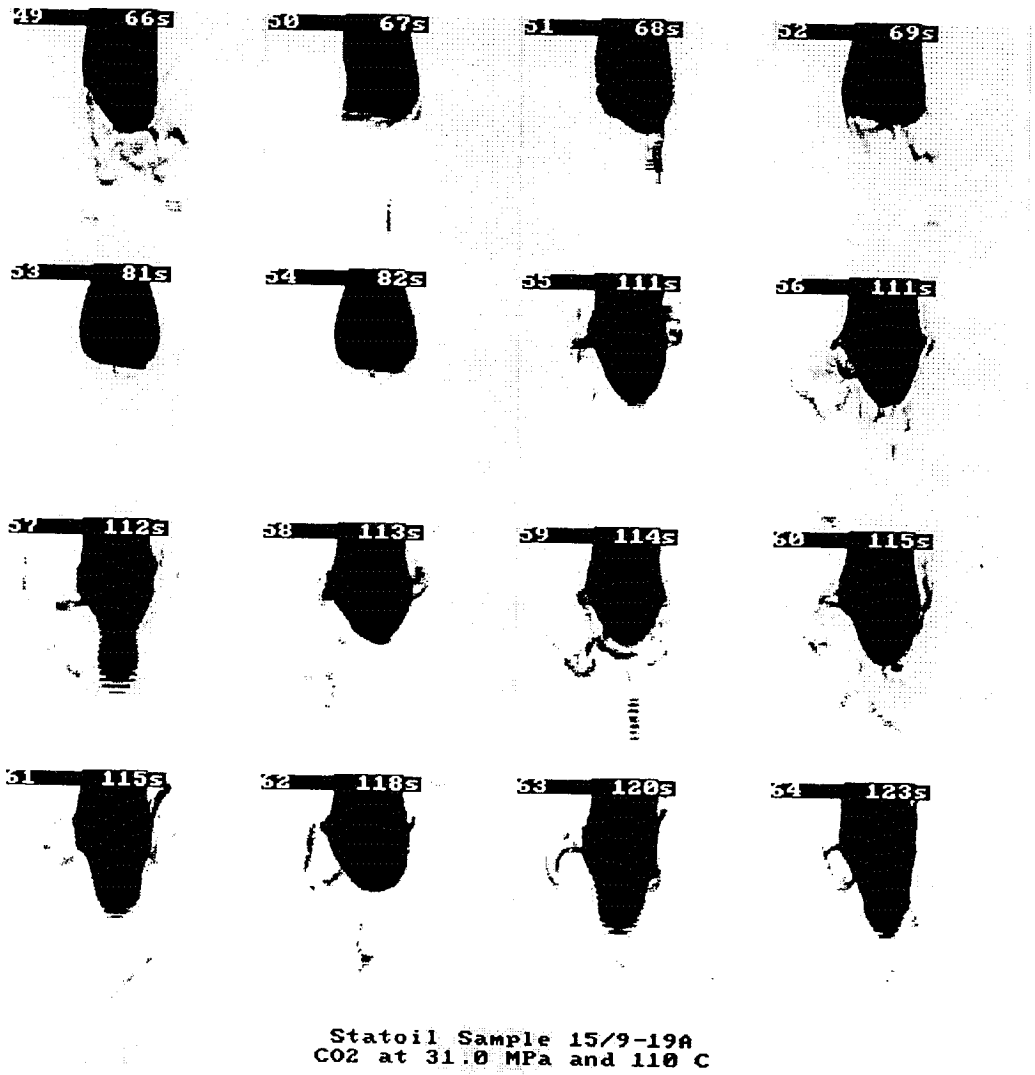
49 66s
50 67s
51 68s
52 69s
53 81s
54 82s
55 111s
56 111s
57 112s
58 113s
59 114s
60 115s
61 115s
62 118s
63 120s
64 123s
Statoil Sample 15/9-19A
CO2 at 31.0 MPa and 110 C

Fig 12 - b

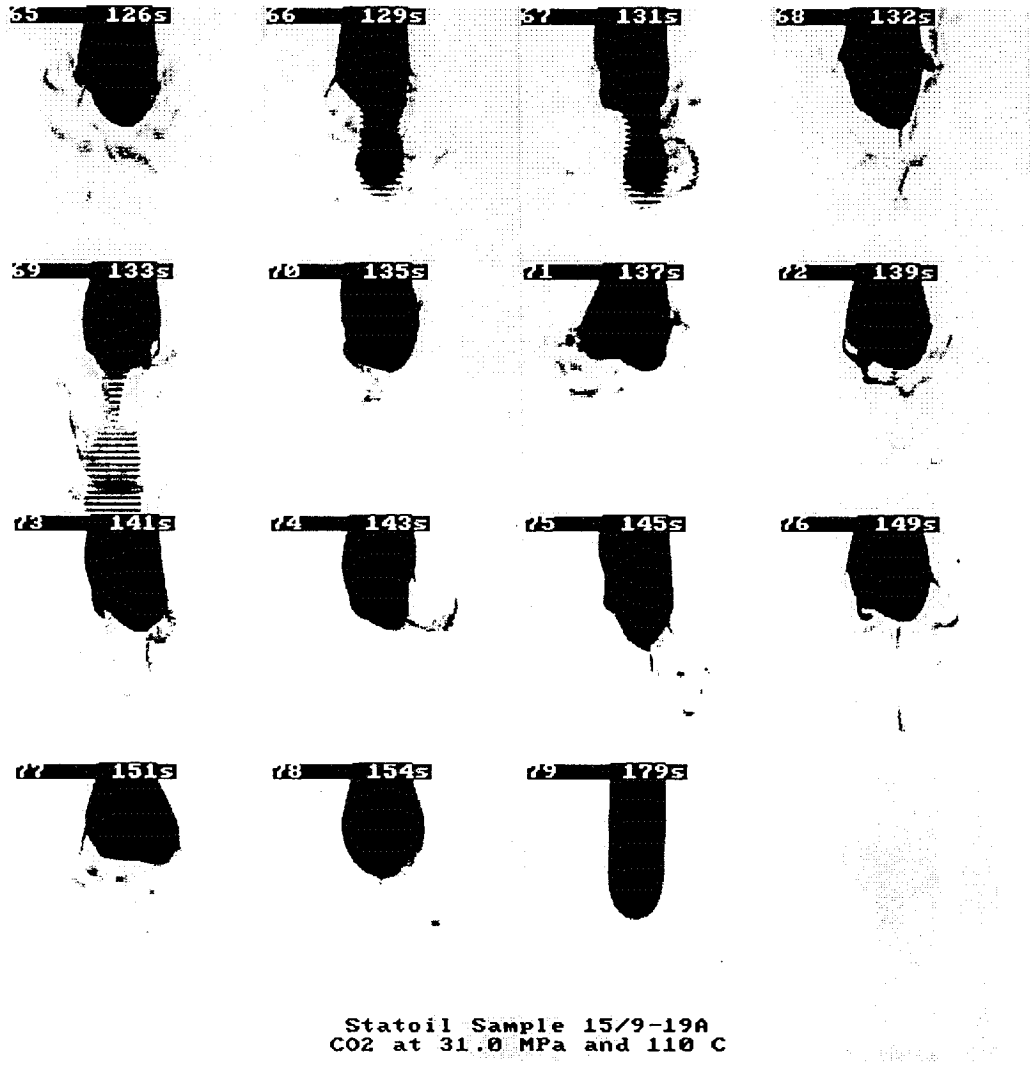
65 126s
66 129s
67 131s
68 132s
69 133s
70 135s
71 137s
72 139s
73 141s
74 143s
75 145s
76 149s
77 151s
78 154s
79 179s
Statoil Sample 15/9-19A
CO2 at 31.0 MPa and 110 C

Fig 13 - b

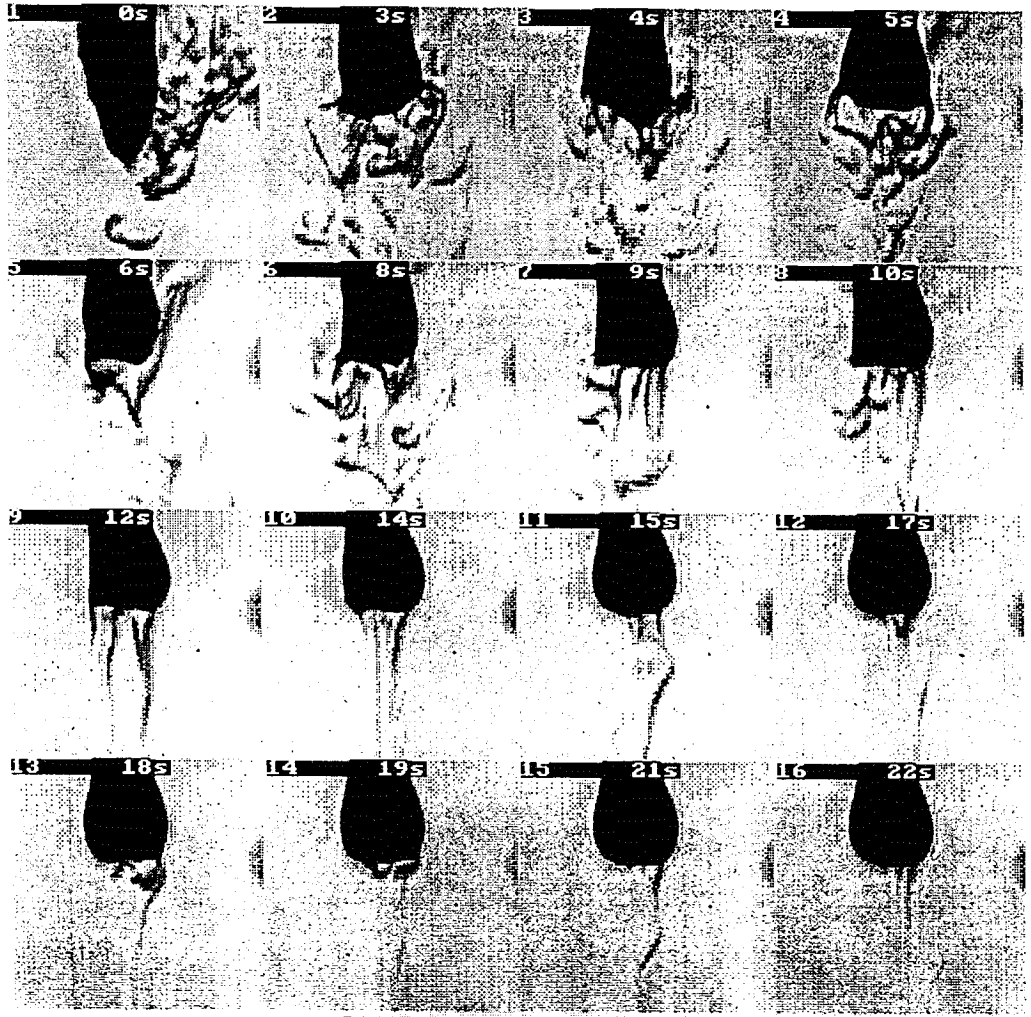
1 0s
2 3s
3 4s
4 5s
5 6s
6 8s
7 9s
8 10s
9 12s
10 14s
11 15s
12 17s
13 18s
14 19s
15 21s
16 22s
Statoil Sample 15/9-19A
CO2 at 31.0 MPa and 110 C

Fig 14 - b

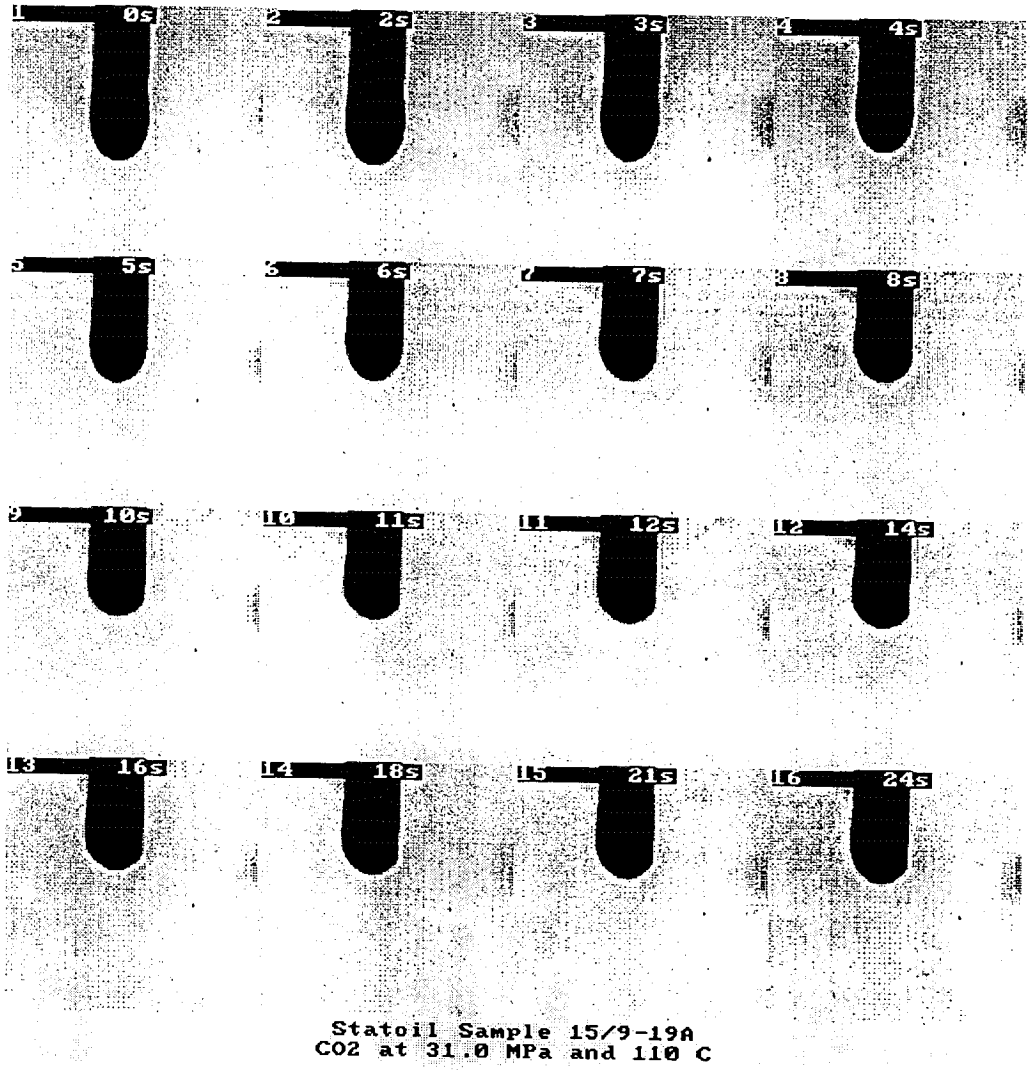
0s
2s
3s
4s
5s
6s
7s
8s
10s
11s
12s
14s
16s
18s
21s
24s
Statoil Sample 15/9-19A
CO2 at 31.0 MPa and 110 C

Fig 15 - b

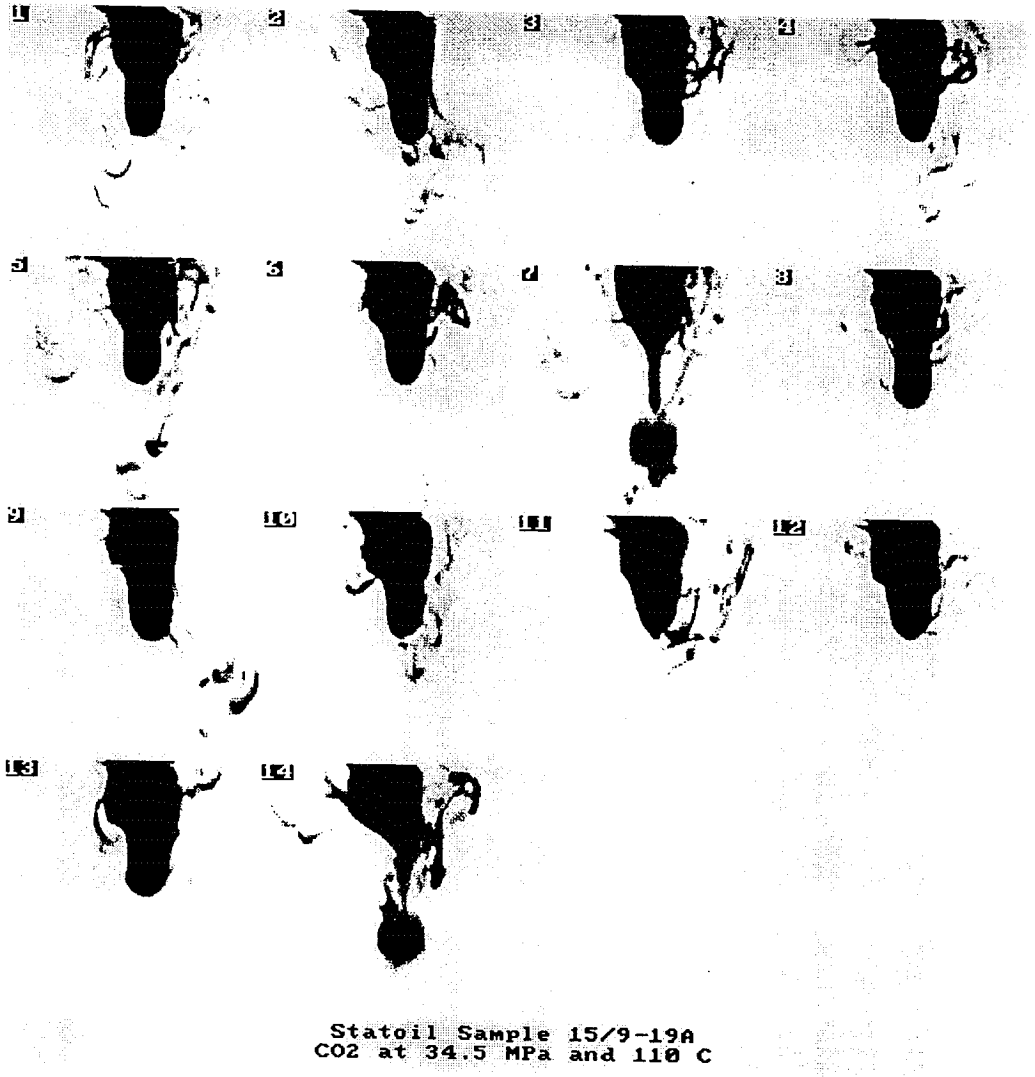

Fig 16 - b